UNIVERSITY
OF OSLO

Master's thesis

Optical Remote Sensing of Glacier Surges in Svalbard

Gabriele Bramati

Geomorphology and Geomatics

60 ECTS study points

Department of Geosciences

Faculty of Mathematics and Natural Sciences

Spring 2023

Gabriele Bramati

Optical Remote Sensing of Glacier Surges in Svalbard

Supervisor:

Andreas Max Kääb

Abstract

Glacier surging is an ice-flow instability that causes surge-type glaciers to alternate between prolonged periods of slow movement (known as the quiescent phase) and brief periods of rapid flow (the surge phase). The occurrence of surging has consistently challenged the idea of normality in glacier flow dynamics, and despite years of research, the mechanisms behind it are still not well-understood. Although only a small fraction (roughly 1%) of glaciers worldwide have been observed to surge, the phenomenon raises questions about the extent of our knowledge about glacier dynamics. In addition, they constitute a natural hazard, as several surges in the past resulted in infrastructure damage, floods, and casualties. In this sense, studying the temporal and spatial variability of surging and fast-flowing glaciers adds to the comprehension of the mechanism regulating their dynamics and evolution through time.

The work presented here focuses on two tidewater fast-flowing glaciers in Kongsfjorden, Svalbard. Kronebreen is a surge-type glacier that has been observed to surge in the past, whereas Kongsbreen is a fast-flowing glacier that has not been observed to surge. This thesis aims to investigate their spatial and temporal variability in surface speed between 2017 and 2021, using optical satellite data (Sentinel-2 L1C product, near-infrared band). At the same time, the performance and challenges of optical feature-tracking in the Arctic are pointed out and discussed.

A feature tracking technique is used to estimate glaciers' surface speed through time and space. In principle, a small subset (or chip) of the image at time 1 (t1) is looked for in a portion (search window) of the subsequent image at time 2 (t2). A normalized cross-correlation matrix is constructed based on grey values of the images. The displacement is computed based on the location of the peak correlation.

Velocities have been found to vary broadly within the season. Kronebreen speed ranges from 1.5 up to 5.6md^{-1}. Speed-ups occur typically in June-July with higher speed-up rates in the first 4 km from the front, after which a sharp drop in velocity has been found going up the glacier. In contrast, Kongsbreen shows lower velocities, ranging from 0.5 to 2md^{-1}, with speed-up timings similar to Kronebreen. Front fluctuations of both have been digitized, and glaciers lost area at a rate of 0.75 km^{2}yr^{-1} and 0.087 km^{2}yr^{-1}

(87'000 m^2yr^{-1}), respectively. Speed maps have been validated using stable ground areas and a temporal triangulation technique. The triangulation assumes that the sum of displacements from two subsequent pairs equals the displacements computed between the first and third images. Comparing our results with previous studies leads to stating that Kronebreen is accelerating its flow, whereas Kongsbreen is moving at the same pace as found previously.

Optical feature tracking limitations in the Arctic have also been discussed. Issues arise firstly by snow cover changes. Other factors limiting the performance of the technique are cloud cover, shadows, appearing and disappearing features in the scenes (such as lakes, crevasses, and medial moraines), lack of trackable features, coregistration errors, and of course polar night, or shallow sun angles.

This work contributes to the monitoring of two of the fastest-flowing glaciers in Svalbard. It proves that optical feature tracking can be used as a complementary source of information to radar tracking (more used in the Arctic) to construct continuous time series of glacier surface speed. This is meaningful in order to improve our understanding of the dynamics of such glaciers, under the framework of the ongoing climate change, especially in the Arctic.

Acknowledgements

I will start by thanking Andreas Kääb for his supervision and for giving me the opportunity to pursue my passion for studying glaciers through satellites. You are the reason why I moved to Oslo since I wanted to learn all I could from you. Thanks for the highly valuable discussions in your office and for the lectures in class.

The experiences in Svalbard, Japan, and in the Norwegian mountains would not have been possible without the connections provided by the University of Oslo, which I deeply thank for making these striking experiences happen.

Oslo is the city where I got to know you, Kaat. Who thought we would have ended up in such a relationship, after meeting on Preikestolen? You took so much time off this thesis and other exams, as well as tears on those countless goodbyes at airports. Instead, you replaced that with lots of fun, laughs, amazing places visited, and love. Your presence simply made me joyful and relieved from challenging moments, even though I rarely fully understood it while I was living it. As I told you many times, I believe the best is yet to come. For now, I deeply thank you for what has come already, and for all you already gave me.

Oslo gifted me with one of the funniest periods in my life, which were deeply influenced by you, Marco, and Davide. Along with "In a good way", BI people, and interconnected friends, countless unforgettable moments marked our time. I did not only find two friends, but two brothers. Also because you actually slept in my brother's room for several nights after Oslo, which makes the previous statement less romantic and more factual. Riccardo and Simo, yes, you are here as well. When most of the people mentioned above left, you took me into your group, along with Cosimo, and brought me into your crazy and funny world. My love for La Zanzara would never be this much if it was not for you, Italiani! Thanks to all of you for making this period one of the best of my life.

Inside the University walls, special fellows deserve to be specifically mentioned. Milot, Femke, Satu and Saskia. Whenever I will hear or think about Oslo again, my thought will be directed to you. Moving to another city does not make it easy to deeply connect with someone and build profound connections. But I can tell you made it easy and truthful. I know Graduation day is not the last of our friendship, and I am grateful our paths crossed, coming from highly diverse and far countries.

"The Boys", the other people sharing our office, and my team OSI Basketball, fulfilled my breaks, weekends, and evenings. You guys have been tough, Norwegian is such a hard language you know?! After fights to make you talk in English, I can say I have built a small (or big?) family in Oslo. Thinking about you will always put a big smile on my face. I wish all of you the best for your future, and here again, I know we will somehow manage to meet. Ah and...do not forget that Italy is the best country in the world!

The second year of this MSc has been specially marked by you, Mathias. Finding such a flatmate is something I wish everyone to experience, and I truly thank you for our very deep talks in moments when the base bricks of my adult life have been put down. Will miss making you coffee or food on tough Sunday (or often any other weekday) mornings. I will keep forever in mind the image of your disgusting Toyota, but what a lovely car...

Will make the rest in Italian for loved ones at home.

Un pensiero va anche ai miei amici di Monza. Scusate se a volte non capivate dove fossi, a tratti non me ne rendevo conto manco io. Una cosa però è certa: io sapevo dove foste voi. Sapere di avere un porto sicuro da qualche parte nel mondo non è scontato quando si sta lontano da casa per tanto. E tornare nel mezzo di questo percorso mi ha sempre dato tanta felicità. Fatico e descrivervi la gioia che ho provato ogni volta che ho avuto la possibilità di riabbracciarvi e sentire il vostro calore. Ora sono molto più vicino fortunatamente, e vi prometto che mi vedrete con più continuità.

Per concludere volevo rivolgere il ringraziamento più grande alla mia famiglia. Mamma, Papà, Davide e Nonna Rita. Con la mia partenza e la nuova vita di Davide ci siamo un po' scomposti, e non penso sia stato facile per nessuno. Quello che però si capisce quando ci si allontana é l'importanza di ciò che si lascia. Bhe, tra un volo e l'altro della mancanza l'ho sofferta diverse volte, ma mi ha fatto capire davvero il vostro valore, spesso dato per scontato. Se ho voluto cogliere questa occasione e lanciarmi é stato anche per voi. Mi

avete dato, oltre alla possiblità, anche la spinta per farlo, senza pormi limiti...anche se per la nonna ero un po' oltre il limite geografico. Invece, mi avete portato a inseguire quello che io vedevo come il successivo passo nel mio percorso. E a vedere come si è evoluta, probabilmente è stata la cosa giusta. Mi auguro di avervi resi orgogliosi di me almeno la metà di quanto sono io nel chiamarvi "Famiglia".

Contents

List of Tables

List of Figures

Chapter 1

Introduction

1.1 Motivation

Polar regions are facing changes from climate change at rates and magnitudes that are among the strongest on the planet (Constable et al. 2022). Starting from the beginning of the 20^{th} century, mean annual air temperature is rising by 1.7°C per decade, leading to a consistent ice loss (Nuth et al. 2010). It has been computed that Svalbard glaciers have experienced a -0.28 myr^{-1} water equivalent area-normalized mass balance for each 1°C increase in mean summer air temperature in the 1936 - 2010 time span (Geyman et al. 2022). As a result of negative mass balance, glaciers, together with ice sheets, contribute to sea-level rise (Zemp et al. 2019).

Svalbard glaciers cover 57% of the total archipelago land area, constituting 10% of the glacier area in the Arctic, excluding the Greenland Ice Sheet (Nuth et al. 2013). Of these, 60% of the total glacierised area is characterized by tidewater glaciers, among which are Kronebreen and Kongsbreen (Błaszczyk et al. 2009). In addition, these two glaciers are among the fastest flowing in Svalbard (Schellenberger et al. 2015). Kronebreen is also a surging glacier since it has been observed in the past (Lamont and Livesay 1876), whereas Kongsbreen has not been observed to surge.

Surging and fast-flowing glaciers have unique scientific importance. Their mere existence raises questions about physical processes controlling fast and slow flow. By studying them, it is possible to identify these processes and learn the instabilities' triggers. Meanwhile, they question what "normality" is in glacier flow.

Schuler et al. (2020) suggested some key research questions related to surging and fast-flowing glaciers, identifying them as "imperative" to be answered. Among those, one is: "How do dynamics and geometry of Svalbard glaciers respond to climate change?". At the same time, they suggest studying unstable glacier flow to address the question.

It is therefore important to fully understand the dynamics of glaciers and keep them monitored in the context of climate change, more importantly in an area that is closely facing its consequences. The current work aims at adding data to answer these questions, and it contributes to glacier monitoring.

The Kongsfjorden–Krossfjorden system is in this respect a very suitable site, being recognized as an "ideal natural laboratory" to study the effects of climate change (Wiencke and Hop 2016). The focus is on the surface velocity of two main tidewater glaciers in north-western Svalbard, flowing into the eastern end of Kongsfjorden: Kronebreen and Kongsbreen. Both are among the fastest-flowing glaciers in Svalbard (Schellenberger et al. 2015).

1.2 Goals of the study

The study focuses on exploring the spatial and temporal variability of two fast-flowing glaciers' surface velocities of Kronebreen and Kongsbreen making use of optical remote sensing data from the Sentinel-2 mission by the European Space Agency (ESA). Five summer seasons (2017 - 2021) have been selected as a study period. The measured speed will be compared to what has been reported in previous literature to assess trends in dynamics. To analyze the surface speed spatial and temporal variability, surface velocity maps will be produced. Further analysis of the velocity will be described making use of centerline transects, cross transects, and selected point time-averaged speeds. In addition, uncertainties and method limitations will be pointed out.

1.3 Outline

The presented Thesis is divided into 6 main chapters. Chapter 1 provides the motivation behind this study and its main goals. Chapter 2 gives a broad overview of surging glaciers, along with principles about glacier dynamics and surface velocity, and a review of remote sensing techniques to study surging glaciers. A description of the study site is

given in Chapter 3. The satellite data used and the technique used to derive glaciers' surface velocities are explained in Chapter 4. Chapter 5 describes the obtained results for both study glaciers. Chapter 6 will discuss the temporal and spatial evolution of glaciers' measured velocities and their accuracy, as well as the method's limitations and advantages. Finally, Chapter 7 summarizes the findings of this study and suggests future developments in the field.

Chapter 2

Background

2.1 Overview on surging glaciers

2.1.1 What is a glacier surge?

The first-ever observation of an unusual and sudden glacier advance dates back to the second half of the 16th century. Around 1559, the Vernagtferner in the Ötztal Alps faced a ”catastrophic advance” accompanied by a ”longer time retreat” as described in Hoinkes (1969) (2.1). After that, a larger audience got to know about what was defined as a "galloping glacier" in Time magazine. It was a surge of the Black Rapids Glacier in Alaska, that occurred in 1936/1937 (Truffer et al. 2021). However, glacial speedups had been already reported by Tarr and Martin (1914) after an expedition in southeast Alaska. Many glaciers faced an unexpected advance, which was attributed to the effect of an earthquake. This explanation has subsequently lost credibility because of the 1964 earthquake in Alaska which did not trigger surges (A. S. Post 1965). Nevertheless, this remained the only proposed reason for glacier surges until the great work of Meier and A. Post (1969). Meier was an aerial photographer that used his repeated shots to detect and describe surge-type glaciers. Meier and A. Post (1969) asked the question ”What are glacier surges?”, and their first definition is the base of nowadays surge definition. These glaciers are characterized by alternation between short periods of fast flow and longer periods of normal or slow flow (G. K. Clarke 1976; Raymond et al. 1987; Sevestre and D. I. Benn 2015; Sharp 1985; Truffer et al. 2021). These oscillations appear to be quasi-period. Geological evidence is also related to glacial surges (Lønne 2016).

Figure 2.1: Drawing of the first reported glacier to surge in 1559 in the Austrian Alps. The painting represents what is presumably a surge in the 1678 summer. Vernagtferner advances from the right, coming out of the tributary valley. The Rofen Valley head can be seen at the back. Image from Hoinkes (1969).

Wavy forms of medial moraines can be indicators of previous surges (Truffer et al. 2021). In addition, frontal moraines strongly distant from the actual front may be related to sudden surges if, when dated, they do not align with past cooling events (Reger 1991).

The two phases composing the surge cycle are defined "quiescent phase" and "surge phase" (Raymond et al. 1987). In the quiescent phase, a reservoir area upstream gets mass accumulation whereas a receiving area gets depleted (Sharp 1985). It is important to highlight that these two do not correspond to accumulation and ablation areas (Truffer et al. 2021). The reservoir area, along with increased ice volume, also increases its velocity and the steepness increases as well in a considerable fraction of the glacier length (Raymond et al. 1987). These changes generate alterations in the basal shear stress, being the glacier flow driver (Bindschadler et al. 1977). An increased volume results in

an increased shear stress while the lower part sees little change. Increased shear stress leads to the reactivation of ice. Conversely, the lower glacier remains stagnant (Raymond et al. 1987). Nevertheless, it is not always the case that the surge initiation takes place in the upper area (Sevestre et al. 2018), but differences among different surge-type glaciers will be discussed later.

The quiescent phase can last for several decades before the surge phase undertakes. Velocities in the surge phase can increase up to two orders of magnitude, reaching more than 100 meters per day (Truffer et al. 2021), lasting for a few months or years. Firstly developing upglacier (even though not always, as already said), high velocities propagate also downglacier. The speed change can be up to 3 orders of magnitude. This leads, even though not always, to a strong advance of the glacier front (Sharp 1985). Morphologically, glaciers become heavily chaotic and crevassed.

When the active phase stops, the upper reservoir appears depleted and lowered. This is accompanied by left trim marks and/or stranded ice on the mountain flanks (Truffer et al. 2021). The end of the active phase is also marked by a massive release of subglacial water, affecting the downstream valley or the fjord in which the glacier flows. After the active phase, ice has been placed at a lower elevation. The geometry is therefore not in equilibrium with the climate (Raymond et al. 1987). The total sum of ice volume before and after the surge leaves it with an overall decreased volume (Figure 2.2).

A distinct feature among these phases is that every surging glacier tends to have a constant cycle length (Meier and A. Post 1969), and this duration seems to be proportional to the surge phase lasting (Dowdeswell et al. 1991). These phases also tend to differ for different geographical regions where surges occur. Alaskan glaciers display a shorter cycle length (1 year for the surge phase and around 15 for the quiescent phase) (Kamb et al. 1985), whilst Svalbard glaciers exhibit longer phases (50 to 500 years for quiescent and 3-10 for the surge phases) (Dowdeswell et al. 1991).

2.1.2 Which glaciers surge?

Since the first works (Meier and A. Post 1969), scientists noticed that glaciers showing surging behavior are not randomly distributed. First of all, not all the glacierised areas of the world have some surging glaciers among them (Truffer et al. 2021). They tend to occur in specific regions, where many other surging glaciers are found. In Canada for instance,

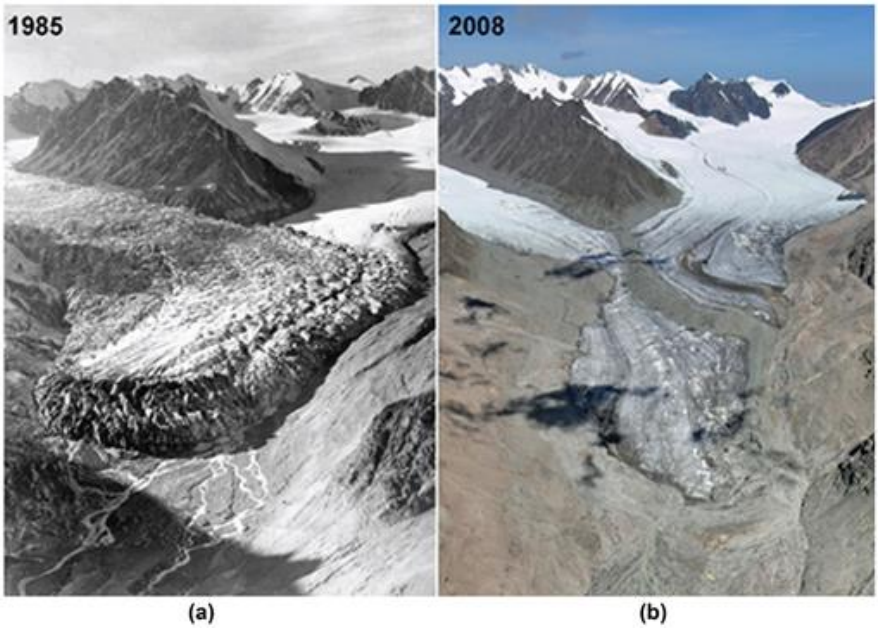

Figure 2.2: Bogatyr glacier, in the Tien Shan massif, (a) during an intense surge phase in 1985 (Institute of Geography Almaty), and (b) decades after (V. Blagoveshchenskiy). Illustration from Mukherjee et al. (2017).

in the Yukon territory, G. K. Clarke (1991) analyzed the geometry of 1754 glaciers, finding that surging and non-surging glaciers have important different geometries. There is a tendency for surging in glaciers that are longer, wider, and less steep. In addition, the presence of subglacial till has been found in many surging glaciers in Svalbard, Iceland, and Yukon, as well as some clusters grouped around fault zones (W. D. Harrison and A. S. Post 2003). Jiskoot et al. (2003) also found that surge occurrence correlates with branchiness and glacier orientation, confirming the low slope factor connection. However, apart from large tendencies, surging glaciers encompass a wide variety of glacier types, including tidewater and land-terminating glaciers, valley glaciers, cirque glaciers, and ice streams (Murray et al. 2003b). In addition, both temperate and polythermal glaciers exhibit surge behavior (Murray et al. 2003b).

Most prominent clusters are concentrated around the following areas: Alaska-Yukon, Arctic Canada, parts of Western and Eastern Greenland, Iceland, Svalbard, Nova Zemlya, and several ranges in Asia among which are Karakoram, Pamir, and Tien Shan (western part) (Sevestre and D. I. Benn 2015). There are also other regions with few surges namely Caucasus, Andes, New Siberian Islands, Kamchatka, and Tibet (Sevestre and D. I. Benn 2015). Svalbard counts a total of 345 surging glaciers, ranking as third among

the areas with the most surging glaciers, after Pamirs (n = 820) and Canada (n = 450). Many studies have investigated common characteristics in these areas, but the climate has not been investigated statistically for decades (A. Post 1969). In 2015, Sevestre and D. I. Benn (2015) compiled a geodatabase of surge-type glaciers and investigated the climatic variables associated with surge occurrence. They found a climatic envelope regulated by temperature and precipitation, which can be subdivided into two zones. One zone encompasses the Arctic Ring, from the Alaska-Yukon, passing from Svalbard and including Novaya Zemlya (excluding Arctic Canada), whereas the other one regards High Mountain Asia. The climatic envelope is characterized by mean annual temperatures between -10°C and 0°C and mean annual precipitations from 30 to 2250 mma^{-1}.

2.1.3 How do glaciers surge?

Surging behavior is very broad and various. A net separation between surge type and non-surge type is not sharp at all (Frappé and G. K. Clarke 2007; Meier and A. Post 1969; Murray et al. 2003b). Mechanisms and dynamics are very different among glacier types.

The first difference between the two surge mechanisms is between land-terminating glaciers and tidewater ones. In the case of the formers', the surge initiates in the reservoir area and then diffuses down the glacier under the shape of a bulge (G. K. C. Clarke et al. 1984). It can be described as a wave of mass that travels with a pace higher than the flow velocity (Figure 2.3). The confine can indicate the transition between warm-based and cold-based ice (G. K. C. Clarke et al. 1984) which is generated by changes in ice thickness.

On the other end, in tidewater glaciers, surges are often started at the terminus and then they propagate upglacier, as seen commonly in Svalbard (Dowdeswell and Benham 2003; Luckman et al. 2002; Murray et al. 2003b; Rolstad et al. 1997). These different surging glaciers also have different cycle lengths between glaciers within a region and between regions (Dowdeswell et al. 1991). For Spitzbergen glaciers, the active phases last around 4 to 10 years, whereas in Alaska, Iceland, and in Pamirs is about 1 to 3 years (D. Benn and Evans 2014). Nevertheless, ice velocities during the surge phase are lower for Svalbard glaciers, with values between 1 to 16 m day^{-1} in comparison to Alaska which could be up to 50 m day^{-1}. This means that for Svalbard glaciers, mass is transferred for a longer

Figure 2.3: Surge bulge at the interface between cold-based and warm-based ice on the Trapridge Glacier (Alaska). Dimensions are in the range of 40m for the bulge height and the width is about 750m. Image from G. K. C. Clarke et al. (1984) taken in June 1980.

time but with lower efficiency. Regarding the quiescent phase, Svalbard glaciers remain stable for 50 to 500 years, elsewhere is around 20 to 40 years (Raymond et al. 1987). In Eisen et al. (2001), it has been described that the surge length is correlated with the time needed by snowfall to fill the reservoir area after a depletion. Therefore, in arid regions, the quiescent phase would be longer (e.g. Svalbard) than for more humid regions (e.g. coastal Alaska). Oppositely, in Iceland, surges occur more irregularly, suggesting the non-unique dependency on climate (H. Björnsson et al. 2003). These properties might also change according to a changing climate (Dowdeswell et al. 1995). Many glaciers that receded to cold-based glacierets, do not have surging characteristics anymore. The same happened for Vernagtferner (Austrian Alps), which surged at different times in the Little Ice Age but is now erased by the list of surging glaciers (Hoinkes 1969).

Temperate glaciers surges

Another difference in the way surges occur resides in the glacier's thermal characteristics. Temperate and polythermal glaciers have different surge fashions. A typical example of a temperate surging glacier is the Variegated Glacier in Alaska, which have long been studied as one of the first monitored surging glacier (Eisen et al. 2001). Throughout the quiescent phase, surface velocities for this glacier increased steadily due to driving stress rise, promoting ice creep (Bindschadler et al. 1977). Sliding contributed minimally to the speedup. Every summer on a part of the quiescent phase, several speedup waves interested the reservoir area, in what was identified as *minisurges* (Kamb and Engelhardt 1987). Waves were coupled with basal water pressure waves, with the same peaks and drops. Kamb and Engelhardt (1987) did not find any correlation with precipitation in these waves, suggesting that peaks in velocity were associated with increased water pressure, maybe released from subglacial storages. Subglacial hydrology, therefore, plays an important role in the surging mode. During the surge, dye studies resulted in indicating a distributed and inefficient drainage system (Kamb et al. 1985), whereas surge termination was followed by a release of considerable amounts of water, suggesting that efficient drainage has been developed. Other Alaskan glaciers have shown a similar way in the surging mechanism (Lingle and Fatland 2003). For Iceland, H. Björnsson (1998) reported a surge in an outlet of the Vatnajökull ice cap in which the velocity speedups migrated both up- and downglacier and analyzed these velocities coincidentally with subglacial lake drainage. He concluded that similarly to other temperate glaciers, the subglacial drainage system has strong differences between active and non-active phases.

Polythermal glaciers surges

On the other hand, polythermal glaciers are characterized by a different thermal structure, in which cold-ice occupies parts of the whole body. It turns out that their surge behavior is different as well. When the cold part is limited, behavior seems to be alike the temperate ones (W. Harrison et al. 1994). When the cold-ice part is more considerate, the surge mode changes. Several studies investigated the surge of Bakaninbreen in Svalbard between 1985 and 1995 (Barrett et al. 2008; Murray 1998; Murray and Porter 2001; Murray et al. 2000) via ground penetrating radar (GPR) and temperature measurements. They showed that cold-ice frozen to the bed was present at the front of the glacier,

whilst the speeding up upglacier was warm-based, thus developing a thermal boundary. The latter propagated together with the bulge during the surge. They also found that sediments were not at melting point in the front, impeding water to flow outwards. This setting leads to an increased water pressure before the front, fostering sliding by lowering frictional strength. The Trapridge Glacier in Alaska, which surged in the last couple of decades of the 20th century, showed a slightly different behavior, for a similar thermal structure (Frappé and G. K. Clarke 2007). Here, a slope steepening developed at the thermal boundary between warm and cold ice. However, the propagation was not concurrent as the thermal boundary moved at a slower rate than the bulge, therefore less influencing than for Bakaninbreen.

Surging models: hydrologic switch, thermal switch, enthalpy

Mechanisms used to explain surges have mainly been two for the last decades (Murray et al. 2003a), even though another model has come up more recently (D. I. Benn et al. 2019). The first proposed one is the *hydrologic switch model* (Eisen et al. 2005; Kamb et al. 1985; Raymond et al. 1987) for temperate glaciers. The model indicates the switch between efficient and inefficient drainage systems as the reason for surge trigger and termination, through changes in subglacial water volume, pressure, and spatial variability. High sliding velocities and low hydraulic gradients allow a stable drainage system. In turn, a high gradient drives cavities to enlarge due to heat production and roof melting being higher than creep closure (Flowers 2015). In winter, water pressure increases due to the closure of conduits created during summer, promoting glacier sliding (Raymond et al. 1987). A hydraulic switch will then be triggered when increasing discharge combines with a basal shear stress threshold being reached (Eisen et al. 2005). In addition, a large volume of water is also necessary to decouple the bed and the glacier itself. It has been proposed that the large amount required might come from a release of englacial storage (Lingle and Fatland 2003), even though there is no credible evidence yet. Also, models are still lacking a sound explanation for soft-bedded glaciers as bedrock-bedded ones (D. Benn and Evans 2014). What is clear and widely accepted in this model is that variations in a subglacial plumbing system do have a close association with surging behavior. However, the actual initiation and termination are not yet fully explained, remaining an open question (W. D. Harrison and A. S. Post 2003).

The second proposed model is the *thermal switch model*, formulated in Murray and

Porter (2001) and Fowler et al. (2001). In polythermal glaciers, frozen and unfrozen conditions coexist, and surges result from changes in these conditions. Being cold-based in lower regions, the glacier has a low speed during the quiescent period. At the same time, the reservoir area builds up ice, increasing stress, and fostering creep rates which in turn results in increased heat production via strain heating. In this positive feedback, some areas of the bed eventually reach pressure melting point. The excessive energy is then used to produce meltwater. As water follows its natural slope gradient path, it encounters the cold-based area towards the glacier terminus. Thus, water is prevented from outflowing, increasing pressure, reducing friction, and promoting sliding. A surge keeps on going until the dissipation of water is allowed, considering that strain heating in the cold-ice leads to reaching pressure melting point.

Different surges on different glaciers can be explained via the two models presented. A need for a unifying theory has been lacking for years, until the work by Sevestre et al. (2018). They presented a one-dimensional theory explaining both surges in temperate and polythermal glaciers making use of enthalpy and mass budgets. Enthalpy sources are found in geothermal fluxes and friction whereas losses are identified in meltwater heat conduction and loss. Surge is therefore triggered when steady states of mass and enthalpy are not reached. Glacier characteristics (climate, geometry, bed) define the possibility to reach a steady state. In the quiescent phase, balance velocities are greater than actual ones and enthalpy is low. It increases due to mass accumulation, as geothermal heating overcomes losses in enthalpy. After a threshold, enthalpy is risen enough to trigger sliding, therefore initiating the positive feedback already explained between frictional heating and sliding, entering the surging phase. The active phase stops once water loss outweighs the production. The model is also able to explain why 99% of glaciers worldwide do not surge. It however needs implementation in more dimensions, meaning that a lot of research still has to be carried out.

2.1.4 Why are glacier surges important?

If we take into account the amount of surging glaciers in the world, one might reasonably ask why are they important if only 1% of the world's glaciers are of surge-type (Jiskoot et al. 1998; Sevestre and D. I. Benn 2015). Many hazards are related to surges, leading to damages and casualties. The following list provides an overview of surge-related hazards and implications, along with examples of damages or casualties that have been reported:

- direct mechanical impact of glacier advance (damage to farmlands and shelters in the Pamirs, Donghui et al. (2016));
- floods directly induced by glacier surge (various glaciers in the Karakorum, Hewitt (2014));
- floods indirectly induced, e.g. river is blocked by glacier advance, with subsequent flooding (casualties, swept away houses, and lost harvest, Yin et al. (2019));
- ice avalanches or glacier collapse (many cases in Kääb et al. (2021));
- glacier travel blockage (in Svalbard for instance, many glaciers are commonly used ways of traveling with snowmobiles. A surge leads glaciers to be intensively crevassed and therefore unsafe or impossible to cross);
- mass balance alterations (a wide range of impacts has been seen on surge-type glaciers mass balance, across different time-scales, King et al. (2021)).

For a more comprehensive and complete list, refer to Truffer et al. (2021).

From the scientific comprehension point of view, surging glaciers raise a lot of questions related to ice dynamics. Why do some glaciers are surge-type and others not? Why do they cluster in some regions? What is the role of the subglacial bedrock or sediment? To what extent do they contribute to sea-level rise? Do they get triggered externally, internally, or by a mixture or both? Is there a single explanation for all surges? Is it possible that glaciers that have never been observed to surge might do so?

2.2 Glacier dynamics and surface velocity

All glaciers move due to the downslope component of gravity or, more specifically, due to the horizontal gradient in gravitational potential which constitutes the driving stress (Veen 2013). The driving stress is matched by resisting stresses including longitudinal stress gradients, lateral drag, and basal shear stress, which act along a surface, in this instance the glacier's bed (Figure 2.4).

Taking into account all the forces, the balance is zero. The resisting force at a given flow depends on ice properties, bedrock or till properties, and glacier geometry (Paterson 1994). The tendency of the glacier is to reach steady-state, like many other entities in nature. Mass is added through snowfall and lost via melting and calving. Ice flow

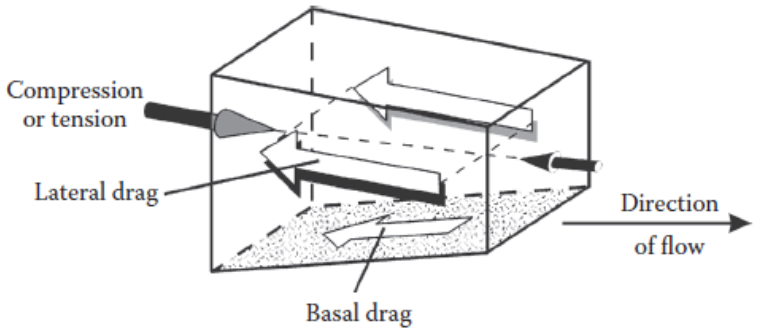

Figure 2.4: Opposing stresses to the driving one (not illustrated). Resistance depends on longitudinal stress gradients and friction generated at the base of the glacier or at the side. Illustration from Veen (2013).

moves mass from an area with snowfall gain to an area with mass loss. Therefore, if the transport is not efficient enough, the glacier will build up mass, increasing thickness and stresses until snowfall rates are matched by transport. This leads to the determination of flux, which is a function of the mass input in the system (in turn defined by snowfall, melt, and geometry) and the outlet geometry (Paterson 1994).

The flow of glaciers is computed via flow laws, which combine the rate of deformation with the stress. The most used one is Glen's flow law (Glen 1955), which has been then adapted by Nye (1957) in the following form:

$$\dot{\epsilon}_{xz} = A\sigma_e^{n-1}\tau_b \tag{2.1}$$

in which τ_b represents the basal shear stress, whereas σ_e the effective stress. n corresponds to an empirical factor derived from lab experiments, which suggests using a value of 3. A is a "softness parameter" (Glen 1955), related to the viscosity of ice, which changes with its temperature, water content, crystal fabric, density, and grain size (Veen 2013). A first implication of the equation is that ice does not deform in a linear way, it is rather identified as a non-linear viscous material (Jiskoot 2011).

The components leading to the surface velocity of a glacier comprise glacier creep, deformation of the basal till, and, the most important for surging glaciers, basal sliding (Figure 2.5).

All three contribute, seldom together, to the total glacier action. However, there are

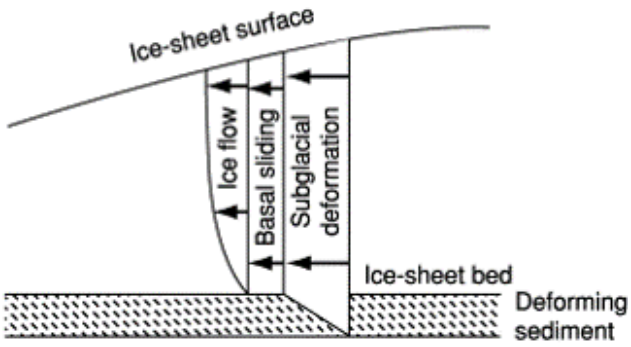

Figure 2.5: Sketch of factors contributing to the total ice velocity: ice deformation, basal sliding, and bed deformation. Illustration from Selley et al. (2005).

differences depending on glacier characteristics. For instance, only glaciers with a bed at melting point (therefore polythermal and temperate) experience basal drag (Jiskoot 2011). On the other end, only when deformable till is present, glaciers do have bed deformation as a component in their flow (Jiskoot 2011). The only factor that is obviously present in all kinds is ice creep. Important to mention is that both sliding and bed deformation are orders of magnitude greater than simple creep velocities (Boulton and Hindmarsh 1987). Velocity at the surface of the glacier (U) results from the sum of all the ice layers, deforming as a deck of cards (Placidi et al. 2006) (U_c), plus the bed deformation contribution (U_d) and the sliding contribution (U_s):

$$U = U_c + U_s + U_d \tag{2.2}$$

They are in turn singularly affected by several factors. Deformation depends on shear strain throughout the glacier thickness, basal shear stress, and coefficients coming from Glen's flow law (Glen 1955). Sliding is influenced by the basal shear stress and the water effective pressure (difference between water and overburden pressure) (Bindschadler 1983). Bed deformation of till can be described as a quasi-viscous flow law, including a constant related to the reference strain rate and one related to the till texture, as well as the stress used as a reference for the shear strain rate (Jiskoot 2011).

In the case of calving glaciers, these factors get more complicated, as there is also water contributing to the complex system regulating ice flow. In fact, basal drag can remarkably affect velocities in the case of water being deep enough to float the ice (D. Benn and Evans 2014). In addition, the presence of water at the glacier front regulates the level

of the entire glacial drainage system, which plays an important role in surging glaciers dynamics, as explained in the previous section (G. K. Clarke 1987).

The glacier velocity regulates the amount of redistribution of mass within a glacier and is a basic process of glaciers (D. Benn and Evans 2014; Paterson 1994; Veen 2013). Changes in speed result in changes in geometry, mass, and elevation gradients. Within the climate change context, it is important to know the velocity of a glacier, as they respond to changes in climate. In fact, it is strongly affected by climatic variables (i.e. melt changes, amount of snowfall, temperature lapse rates), making it possible to use it as an indicator of climate change (Millan et al. 2019). Therefore, it represents a crucial glaciological parameter in glacier monitoring (Kääb 2005b).

2.3 Remote sensing of glacier surges

During the past half century, glacier studies making use of a variety of remote sensing platforms and methods have grown significantly. The first used images date back to the 60s and early 70s with the US Corona program (Raup et al. 2015) which have been used to get glacier extents by later works (Bhambri et al. 2011; Bolch et al. 2010; Narama et al. 2010). Subsequently, a long and consistent program for glacier monitoring came with the advent of the LANDSAT mission, which started in 1972. Many satellites came in the following decades, with different ground resolutions, radiometric resolutions, and spectral bands employment. All these are well summarized in Table 7.1 in Raup et al. (2015). 2013 marked the arrival of Landsat 8 which, due to many improved characteristics such as radiometric resolution, pushbroom principle, improved temporal resolution, and advanced system recording as well as ground download capability (Roy et al. 2014), marked a strong improvement in glacier studies. After that, one of the nowadays most widely used optical system for glacier monitoring is the European Copernicus Sentinel-2 satellite series, launched in June 2015. More details on the mission will come in the following chapter.

The wide acceptance of glaciers as indicators of climate change, the fact that raw data is freely available (e.g., with the opening of the Landsat archive), and the significant effects of their changes on society at various scales (local, regional, and global), are all cause for the rise in glacier studies via remote sensing methods. The remoteness of these natural bodies also leads scientists to find alternative means for their study, as it is very

often the only possible method for this (Paul et al. 2015). The point of view of satellites provides a powerful combination with ground-based observations. Spatial and time scales allow for a comprehensive and wide collection of data, otherwise almost impossible to get from solely ground-based measurements.

The study of surging glaciers' velocity via satellites mainly divides into two main approaches. The first one is exploiting radar wavelengths (e.g. Sentinel-1), whereas the second is by optical missions (e.g. Sentinel-2, Landsat 8) (Sun and Qiao 2021).

2.3.1 InSAR

In relationship to the great elevation changes involved in surging, InSAR provides a powerful tool to study build-up of bulges in the quiescent phase and ice volume changes during active phases (Leinss et al. 2017). Also, surface velocities can be mapped by converting the line of sight velocities into horizontal ones (Goldstein et al. 1993). Its applicability for velocity mapping is however challenging due to seldom steep topography, snow phase changes, and atmospheric conditions variability between two SAR acquisitions (Rao 2011a). In addition, the technique is also strongly affected by layover and shadow in mountain areas (Luckman et al. 2007). It can, however, measure displacements down at the millimeter scale, depending on the temporal difference between acquisitions (Raup et al. 2015). On the other hand, it is affected by upper limits in displacement measurement (Rao 2011b). It occurs when the phase change is the same as the phase sampling rate in range (Vachon et al. 1996). In order to be detectable, the movement has to be less than $\lambda/2$. When it is higher than this value, phase cycles become undetectable on the interferogram, and phase unwrapping becomes not possible.

2.3.2 Radar tracking

Feature tracking can be done both with radar and optical images (Scambos et al. 1992). Co-registration between the input images is needed in either case. In the case of radar use, the matching exploits mainly the intensity of the signal, tracking distinct features (crevasses, boulders, supraglacial lakes, features on the ice, pinnacles, etc.) clearly visible in the image. In some cases, however, the "speckle tracking" is performed. With this technique, rather small features are tracked, being the light-dark patterns found in images due to the phase coherence over stable surfaces in both frames (Strozzi et al. 2002). The greatest advantage of radar tracking is the non-dependency on light and meteorological

conditions (clouds and rain). It can also conduct measurements during day and night, which comes in handy for the polar night at high latitudes (C. Wang et al. 2021). Due to its powerful applicability, many studies have been performed using radar (Leclercq et al. 2021; Luckman et al. 2002; Luckman et al. 2007; Schellenberger et al. 2015).

2.3.3 Optical tracking

In this work, the focus will be put on optical feature tracking. The principles are the same applied to radar tracking. In the use of this technique, the main issues are shadows, snow cover changes, and clouds. Shadows themselves do not create specific problems, as demonstrated by Kääb et al. (2016). Shadow boundaries do however create issues, representing a sharp visual contrast. Snow cover changes lead to high-correlation tracking, as snow patches are very similar, and performing feature tracking in the Arctic involves having snow cover almost all year. Despite radar being generally more used for high-velocity glaciers, several studies have been carried out using optical systems (Beaud et al. 2022; Kääb et al. 2016; Rolstad et al. 1997; Wendt et al. 2017). Specifics on the optical feature tracking functioning and limits will be explained in the Methods chapter.

2.3.4 Further techniques for surges detection and monitoring

Surging glaciers can be identified and monitored in many different ways apart from optical feature-tracking. As explained, feature tracking can also be done using InSAR and SAR tracking. Leclercq et al. (2021) used radar backscattering and Normalized Difference Index (NDI) to detect intense crevassing over glaciers, based on the fact that radar backscattering increases significantly during a surge. Ingólfsson et al. (2016) investigated the geological record in the forefield of glaciers using remote sensing techniques. Another geological feature common in surging glaciers is looped moraines. Herreid and Truffer (2016) monitored the shifts in looped moraines via automated identification to detect flow instability. DEMs are also useful to compute the mass transfer during a surge from the reservoir to the receiving area (Singh et al. 2021). Paul et al. (2022) among many aspects, also used glacier length variations to monitor glacier surges, whereas Z. Wang et al. (2023) monitored the bulge front propagation.

Chapter 3

Study area

The study area in this work focuses on two glaciers located in Kongsfjorden (79.91°N, 12.51°E), north-western Svalbard, namely Kronebreen and Kongsbreen (Figure 3.1). The selected area includes also the front of Kongsvegen, which is an almost stagnant glacier flowing as well into Kongsfjorden. The focus is however put on the two dynamic glaciers, being among the fastest flowing in Svalbard (Schellenberger et al. 2015). In the first section, an overview related to the fjord will be given. Afterwards, each glacier's characteristics and surging history will be described.

3.1 Kongsfjorden overview

Kongsfjord is located in northwestern Svalbard, close to the Ny-Ålesund research station. The basin is around 1430 km^2, of which more than 70% is covered by glaciers (Scholzen et al. 2021). The fjord bathymetry is rather complex and non-uniform, with depths ranging from 400m in some areas and <60m at the head (Trusel et al. 2010). Both a high spatial and temporal dynamism of marine processes characterizes the fjord, resulting in a high seasonality also found in many Arctic fjords (Syvitski 1989). Weather in this area is very variable, given the geographic position of Kongsfjord. It lies between the Greenland East current to the North-West and the Norwegian Atlantic current to the South (Ingolfsson 2000). Kongsfjord shares some traits with large fjords and others that are unique to Arctic ones (Svendsen et al. 2002). With the formers, it shares the supply of freshwater and the seasonality behavior, with specific wind directions that impact stratification and circulation (Farmer and Freeland 1983). On the other end, Arctic fjords

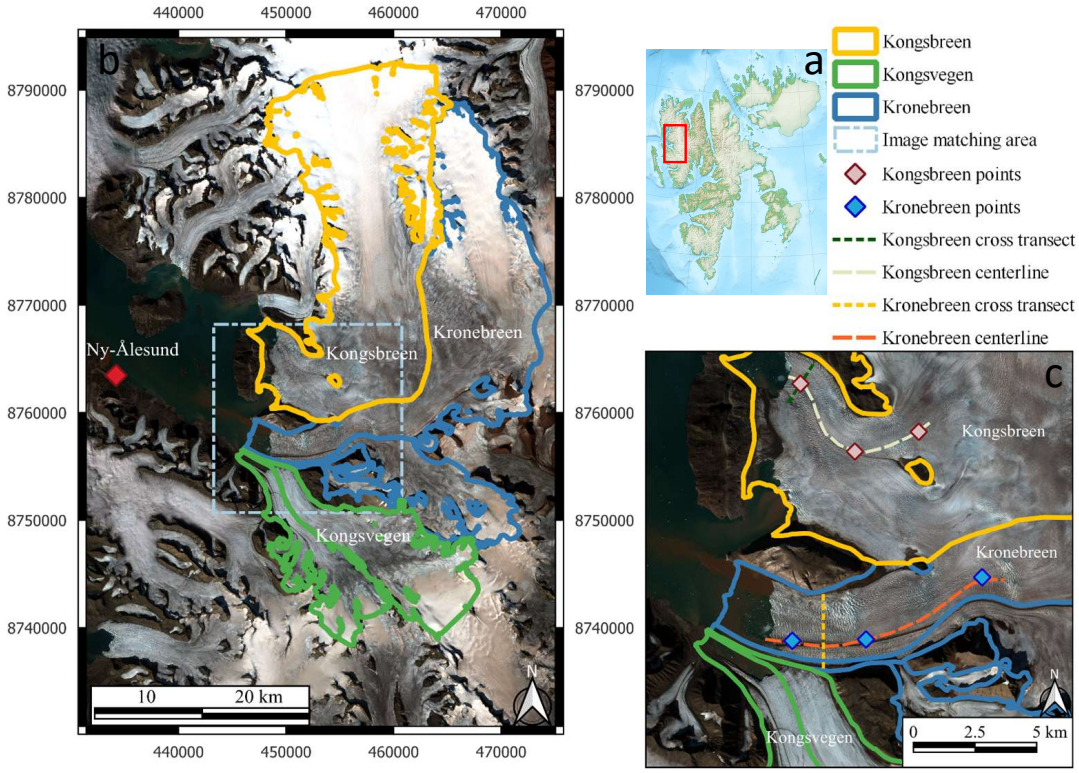

Figure 3.1: a) Location of the study area relative to the Svalbard archipelago. b) Overview of Kongsfjorden. c) Subset used for image matching. Glacier outlines are taken from the Randolph Glacier Inventory 6.0 (https://www.glims.org/RGI/). Cross transects, centerlines and singular points (front - mid - up) to compute time-averaged velocities have been placed manually.

are distinguished by how freshwater enters the fjord system, coming as glacial meltwater and icebergs from calving glaciers. Fast ice freezing and melting, which occur in the inner part of fjord arms, affect the fjord dynamics in two ways: by removing freshwater from the surface layer and replenishing when freezing and melting occur, and by mixing water masses as a result of vertical convection caused by salt rejection during freezing (Svendsen et al. 2002). A tectonic boundary between the Northwestern Basement Province of Svalbard and the fold-thrust belt system from the Tertiary underlies Kongsfjorden (Bergh et al. 2000). Phyllite with embedded quartzite layers, mica schist and marble compose the bedrock in this area (Norwegian Polar Institute).

The climate is dependent on atmospheric circulation, light conditions variations (e.g. polar night), sea ice spatial and temporal variability, and ocean circulation patterns. The Icelandic Low and the Greenland-Arctic Ocean High regulate the large-scale circulation. These pressure zones push warm and humid air from the South (North Atlantic) to

the Norwegian Sea and the Barents Sea. The considerable difference in the air masses involved results in sharp weather variations, particularly in winter (Førland et al. 1997).

Radiation throughout the year is characterized by a strong seasonal variation. The polar night begins on the 25th of October and ends on the 17th of February. Conversely, the polar day period goes from April 18th until August 24th. In Spring and Autumn, twilight typifies days. The greatest irradiances are recorded in July and August (Hanelt et al. 2001). On days with high solar zenith angles, the surface energy balance and heat available are strongly controlled by latent heat. On the other hand, in summer, the shortwave radiation plays a major role.

Sea ice in the fjord has been reported to last from April until July in the late 20th century (Svendsen et al. 2002). However, in recent years, it has faced a clear decline both in thickness and extent (Pavlova et al. 2019). Calving glaciers in the fjord generate icebergs, which are composed of meteoric ice and are mixed with sediments and ice-rafted debris. The released sediments also affect the albedo of sea ice and its mechanical and melting processes (Svendsen et al. 2002). Once the sea ice melts in Spring, sediments both embedded in the sea ice and the ones coming from glacial meltwater alter the suspended load in water (Beszczyńska-Möller et al. 1997). The amount of particulate then has consequences on several aspects of the fjord as the euphotic zone extent, heat transfers, living organisms, and seafloor properties (Sexton et al. 1992).

3.2 Glaciers geometry, characteristics, and dynamics history

3.2.1 Kronebreen

Kronebreen is the outlet glacier of two main catchments in Kongsfjord. The bigger one is Holtedalfonna, which stretches East and North from the calving front, whereas the smaller one is Infantfonna, towards the South-East (Figure 3.1). The total area covered by the two systems adds up to 373 km^2 and develops from sea level to 1400 m a.s.l. (Nuth et al. 2013). The glacier subglacial topography has been surveyed by Lindbäck et al. (2018), demonstrating that Kronebreen is fully grounded below sea level. It features a highly crevassed surface with various icefalls generating topographic steps. It has a width of $\sim$ 3 km in the lowermost part, which decreases to $\sim$ 1.5 km where it is joined by the Infantfonna catchment.

A first observation on Kronebreen has been noted by the Lamont expedition (Lamont and Livesay 1876). Here, a prominent surge in 1869 (or the year before) is described, where the glacier reached its maximum extent (Liestøl 1988).

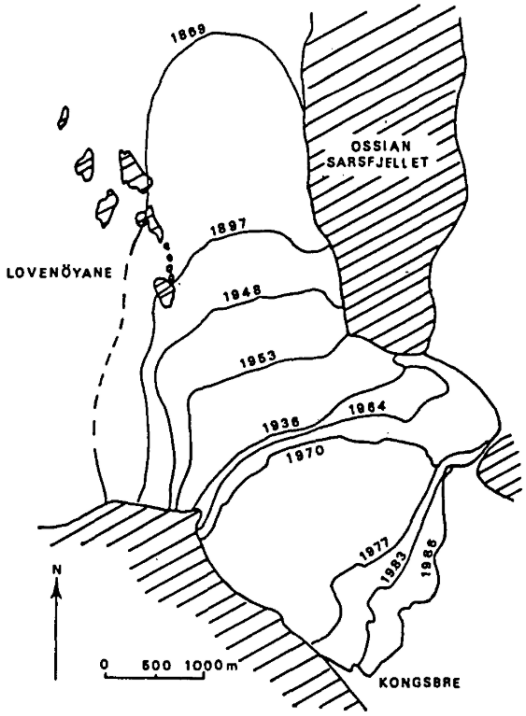

Figure 3.2: Map of the 1869 Kronebreen surge in Kongsfjord as mapped by Lefauconnier (1992).

After that, until 1995, it started to retreat towards the West (where the catchment area is) for about 11 km (Svendsen et al. 2002). Kronebreen's southern neighbor, Kongsvegen, is also a surging glacier. Nowadays its dynamic is stagnant, but it has surged in the past. The retreat phase of Kronebreen stopped due to a surge of Kongsvegen in 1948. Its advancement was less extensive than that of its neighbor, with a calving front advance of 4 km towards West-Northwest (Melvold 1998). Back then, the two glaciers had a single shared calving front. Throughout the following years, Kongsvegen retreated more than Kronebreen and is nowadays moving a few meters per year (Nuth et al. 2012). It is now in its quiescent phase, and significant build-up of mass up-glacier and surface steepening is being observed (Nuth et al. 2012). Given the strongly different velocities, their appearance is also very diverse (3.3).

Kronebreen, like other glaciers in the fjord, is polythermal (H. K. Björnsson et al. 1996). Temperature is in the proximity of pressure melting point, therefore liquid water is present all year round (Sevestre and D. I. Benn 2015). It is characterized by clear

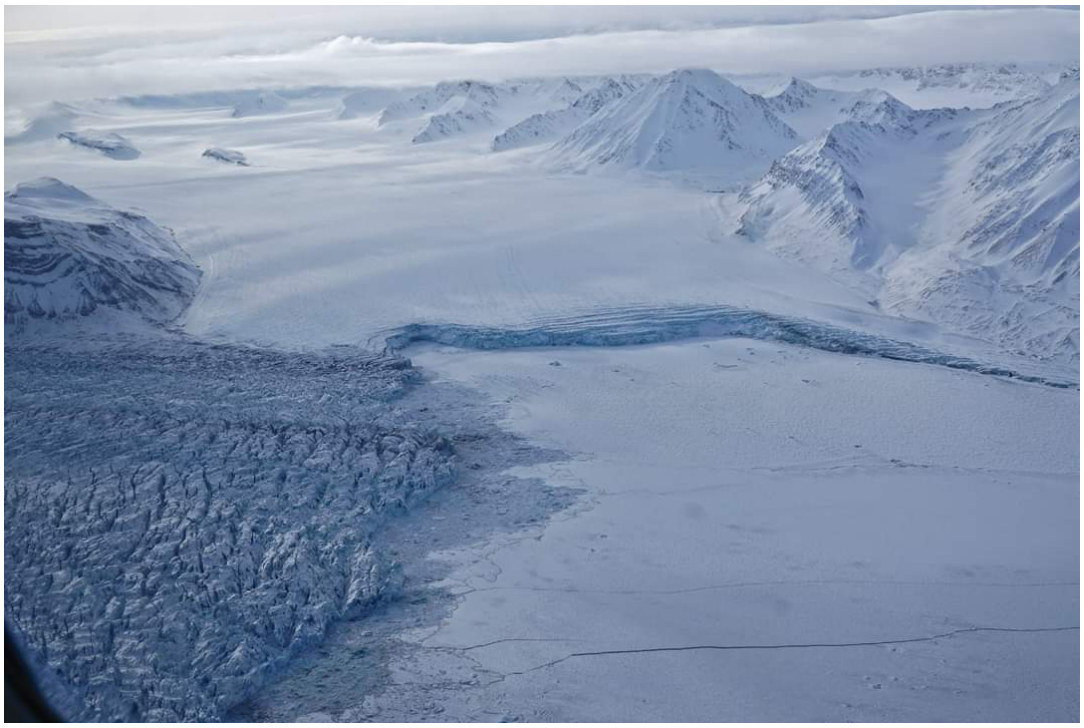

Figure 3.3: Aerial photo of the front of Kronebreen and Kongsvegen in April 2022. Credits: Emilie Nicholls

seasonal flow variations. Speed starts to increase in early Spring (March, April) reaching maximum velocities in late summer (August, September), following the timing of melt season (Scholzen et al. 2021). The input of water to the basal system of the glacier seems to play a crucial role in flow velocities. Schellenberger et al. (2015) found that a considerable part of velocity variability is controlled by the input of rainfall or surface meltwater to the base, suggesting a basal lubrication mechanism. Vallot et al. (2017) also analyzed high-temporal resolution velocities to estimate glacier base characteristics. They strongly suggest annual flow changes are tuned by subglacial hydrological conditions. In addition, it is crucial in combination with bedrock topography and summer melt to control basal sliding, which is the controlling factor for fast-flowing ice.

3.2.2 Kongsbreen

On the north of Kronebreen, Isachsenfonna feeds the Kongsbreen outlet glacier, with a total area of 378 km^2. In the terminal part, a bedrock ridge causes the glacier to split into two parts (Figure 3.4), Kongsbreen North and Kongsbreen South (Scholzen et al. 2021). The elevation covered is similar to Kronebreen, up to 1400 m a.s.l. (Nuth et al.

2013). The velocity patterns are very different among the two branches. The northern one is fast-flowing, with maximum speeds above 2.5 md^{-1}, whereas the southern part is slow-moving since it is partially land terminating (Schellenberger et al. 2015). Between 1990 and 2007, the northern branch retreated of more than 1.5 km, with considerable thinning of the terminus area (Nuth et al. 2012). For Kongsbreen, there is no report on surging activity in the past years. It however is a fast-flowing glacier.

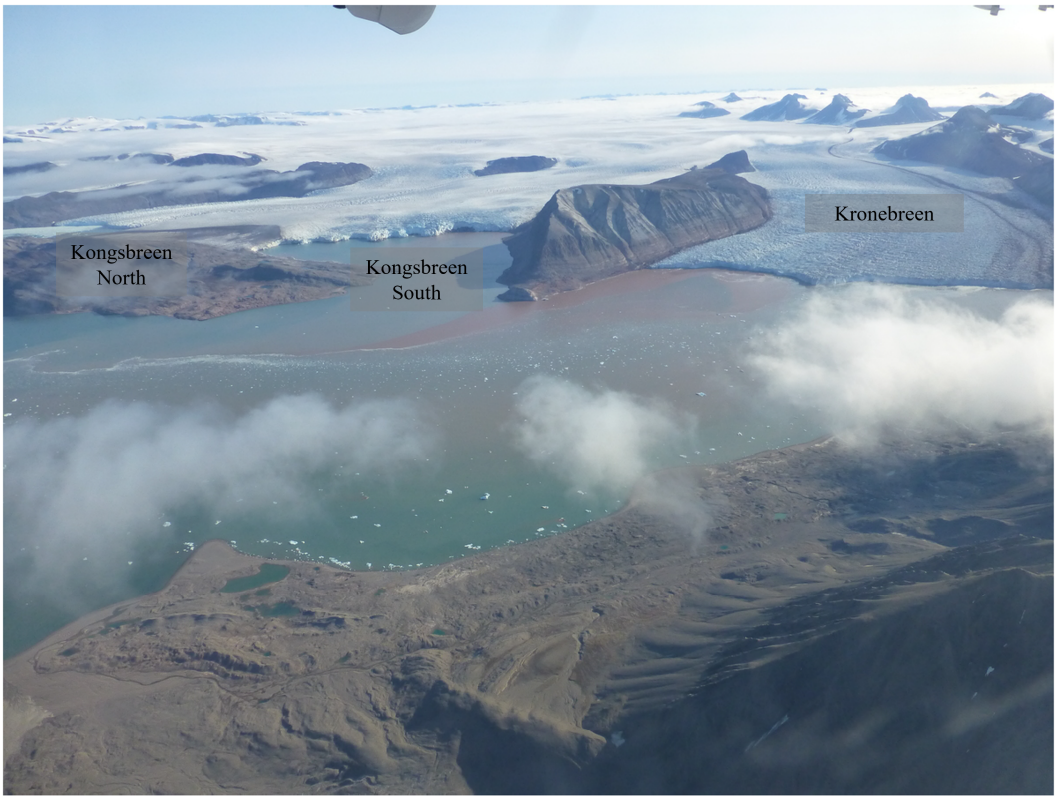

Figure 3.4: Aerial view of the study area in 2016. The two calving fronts of Kongsbreen on the left and Kronebreen on the right. Please note the difference in the glaciers' look, with Kronebreen being far more crevassed than Kongsbreen. Credits: Susan Barr

Chapter 4

Data and Method

4.1 Sentinel-2 platform

The data used in this study is composed only by Sentinel-2 acquisitions. The mission launched by the European Space Agency (ESA) is composed of two satellites, Sentinel-2A and Sentinel-2B. The former has been launched on 23^{rd} June 2015 whereas the second on 7^{th} March 2017. Platforms follow a sun-synchronous polar orbit with a phase difference of 180°. Both have installed the MultiSpectral Instrument (MSI). It generates 12 bit images with 10m spatial resolution for four bands in the visible and near-infrared (VNIR), six VNIR and short-wave infrared bands at 20m, and 3 bands at 60m of which one is in the blue domain and two in the shortwave infrared (SWIR) (Figure 4.1). The mission provides the highest resolution publicly available imagery. The acquisition technique is pushbroom. Revisit time from the same orbit reaches up to 5 days at high latitudes (e.g. Svalbard), on the same orbit. Their orbit is at an altitude of 786 km and they acquire at 10:30 am in Descending Node, providing images with 290km of swath. Processing of data provides products at different levels. The product used in this study is the Sentinel-2 Level 1C, which consists of radiometric corrected Top-of-Atmosphere (TOA) reflectances. Raw granules are mosaicked and orthorectified exploiting the digital elevation model (DEM) PlanetDEM90.

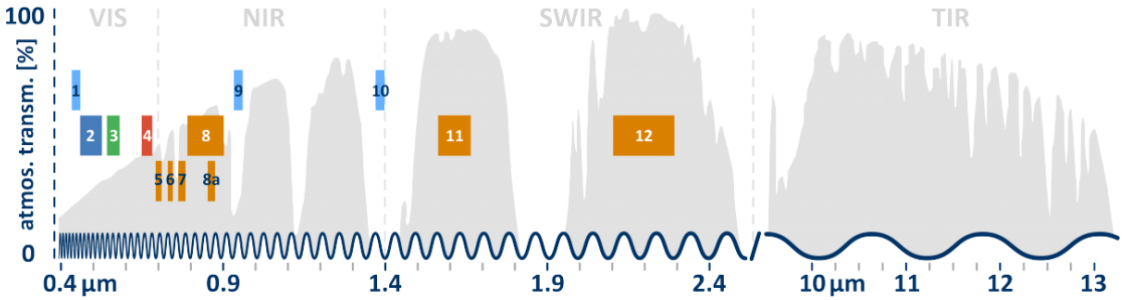

Figure 4.1: Sentinel-2 acquisition channels. Illustration from https://blogs.fu-berlin.de/reseda/sentinel-2/.

4.2 Sentinel-2 band selection

Feature tracking techniques exploit single-channel images. The band selection as input for the feature tracking is therefore an important step, as it might affect the matching (Kääb et al. 2016). Various previous glaciological studies have used near-infrared (NIR) bands, based on ASTER performances over ice and snow (Herman et al. 2011; Kääb et al. 2016; Nagy et al. 2019; Quincey and Glasser 2009. For this study, the L1C product of NIR band 8 (centered at 832 nm with a bandwidth of 105 nm) has been chosen. The ESA Data Quality Report for the MSI instrument states the geometrical and radiometric performance of the sensor. Absolute geolocation has an uncertainty < 11 m at 95.5% confidence whereas the radiometric uncertainty is $< 5\% \pm 2\%$.

4.3 Image selection

The Sentinel-2 images selected come solely from orbit 38, with the ground track passing over the Western edge of Colletthøgda, the elongated land separating the northern part of Kongsbreen and the Southern part of Kongsbreen South, with a Northeast-Southwest orientation. By choosing only data from this orbit, images are assumed to be already coregistered and are acquired with a maximum view angle of around 1.2°. In addition, by taking two optical scenes from the same orbit, orthoprojection errors should be the same in both images used for pair calculation and would therefore be eliminated in the velocity map (Chudley et al. 2022). In addition, out of the whole scene (tagged "T33XVH"), only a part has been clipped for the matching (light blue square in Figure 3.1), in order to speed up the processing.

As already mentioned, the feature tracking algorithm is limited by the presence of clouds. For this reason, out of all the images available for the 2017 - 2021 study period, a manual selection according to the cloud cover over Kronebreen and Kongsbreen has been performed. Despite being time-consuming, it ensures that all the images used for matching are valid and do not need to be filtered afterward for cloud-derived mismatches. However, in order to keep a fair volume of data, few images are partially cloudy over small parts of the glaciers. The choice to keep some of these has been made in order to keep the monitoring as dense as possible for both glaciers. The total number of images is equal to 34. Table 4.1 summarizes the yearly subdivision of the selected images, as long as the first and last image date per season.

Table 4.1: Sentinel-2 scenes selected for the study period

	2017	2018	2019	2020	2021
Images n.	4	6	11	5	8
Start date	15^{th} April	5^{th} April	2^{st} March	30^{th} March	14^{th} April
End date	29^{th} July	17^{th} Sept	17^{th} Sept	7^{th} August	11^{th} Sept

4.4 Feature tracking technique

To derive surface velocities between the selected Sentinel-2 pairs, a ”feature tracking” (or ”image matching” or ”template matching”) technique is employed. The technique is explained in many papers and books. What is explained hereafter is mainly taken from Kääb and Vollmer (2000). The whole algorithm has been coded in Python 3.6 making use of PyCorr as the core step, which performs the actual image matching. A schematic view of the procedure is illustrated in Figure 4.2.

In this technique, the entities that are looked at in the pairs are sub-areas of the gray-level scenes, referred to as ”reference block” (or ”template”). The idea is to look for the sub-area distribution of gray levels in the second image. Since this process is computationally expensive, the ”reference block” is looked into the other image only for a part of it, called ”search window’ or ”search/test area”. The corresponding ”reference block” in the second image is called ”test block”. The comparison can be assessed in many ways. Double

cross-correlation is the most common criterion, nonetheless, the one used in this work. The equation (Eq. 4.1) allows to identify corresponding image chips in the selected image pair, and makes use of the grey values in the images:

$$\Phi(i,k) = \frac{\sum_j \sum_l s[(i+k,k+l) - (T_{test}/N_{test})] \times m[(j,l) - (T_{ref}/N_{ref})]}{\sqrt{\sum_j \sum_l s^2[(i+k,k+l) - (T_{test}/N_{test})] \times \sum_j \sum_l m^2[(j,l) - (T_{ref}/N_{ref})]}} \quad (4.1)$$

In Eq. 4.1, Φ corresponds to the double cross-correlation function, (i,k) and (j,l) refer to the coordinates of the reference and test block, s identifies the grey-value function of the test block, $s(i,k)$ is the grey value at (i,k) coordinates, m same as s but for the reference block, $m(j,l)$ refers to grey values at (j,l), the two T are the sum of reference values for test and reference, the two N are the total number of pixels for both test or reference, since they are the same. The location of a distinct maximum in the double cross-correlation function is used to identify the block movement (see arrows indicating the peak in Figure 4.2.

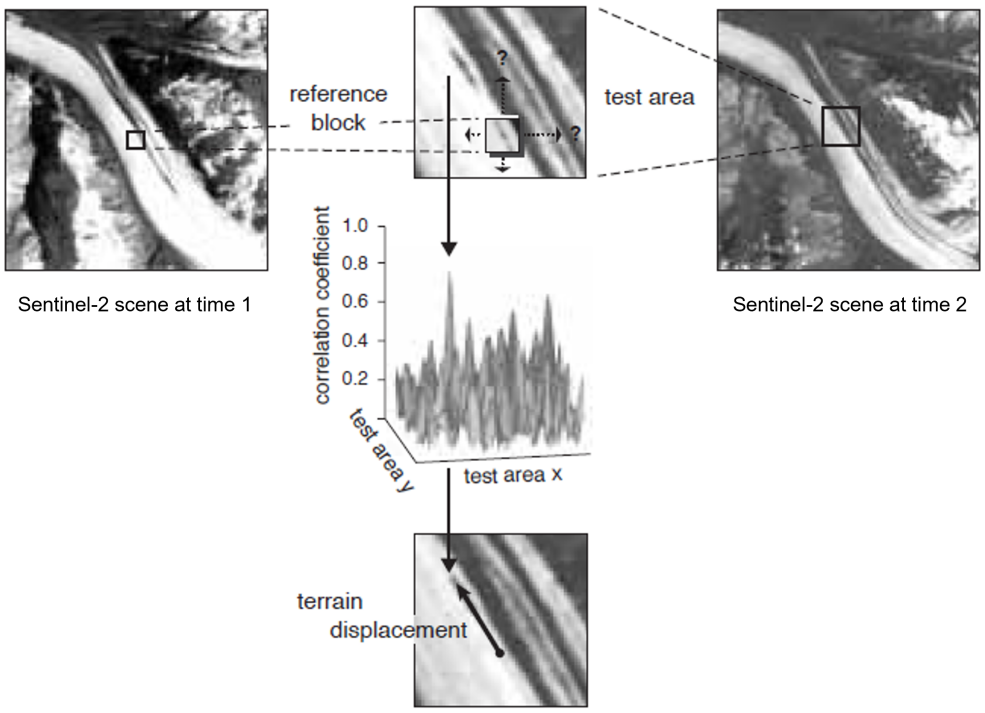

Figure 4.2: Schematic illustration explaining the "feature tracking" technique. Modified from Kääb (2005a)

The chosen template size in this work equals 11 pixels (i.e. 110m) following a previous paper in the same area (Kääb et al. 2005). In that study, only Kronebreen was analyzed.

The dimension of the ”reference block” can infer on the results, therefore the choice has been made in order to consistently monitor the glacier speed. For the search window, a novel technique has been explored which has been called "adaptive search window". After a first try with a visually inspected search window (simply by image flickering), it has been seen that summer velocities are around 6 md^{-1}. Therefore, this velocity has been multiplied by the difference in days between consecutive pairs, and again multiplied by two. This means that each pair has the same template size but a different search window, adapted to the number of days separating each couple of scenes.

However, a larger search window also means more computation cost. Some other tries have been made to reduce it, from simply multiplying the 6 md^{-1} times the days difference to get the search window (therefore without further doubling it), and by increasing it by 30%. In both cases, many pixels were not matched in the fastest areas of Kronebreen (the fastest of the two), suggesting that the template has moved by a greater distance. The search window however does not influence the velocities computed, but it rather increases the chances for a mismatch, given the fact that a greater area is surveyed for finding the template. More on the method limitations will come in the discussion part.

Even though not applied in this work, it is worth mentioning that some authors make use of various techniques to improve the matching performance. Fahnestock et al. (2016) and De Lange et al. (2007) use a high-pass filter in order to isolate glacial surface features and improve movement retrieval. Principal Component Analysis (PCA) is also exploited in multispectral images (Scambos et al. 1992), whereas edge detection techniques (Ahn and Howat 2011) are used to enhance crevasse limits which constitute the optimal feature to be tracked on a glacier.

4.5 Postprocessing

Once the image matching has been performed, the resulting displacements have been filtered in two steps. First of all, a filter on the maximum correlation has been applied ($\Phi > 0.5$). Other works use higher peak correlation thresholds (Kääb et al. (2005) and Kääb et al. (2016) use 0.6 for instance). The choice of the threshold is highly dependent on the images available, local conditions, snow conditions, the purpose of the study, and other local variables. In this case, the choice of 0.5 has been made in order to keep most of the computed displacements in order to identify where optical tracking faces the most issues.

For different purposes, a higher value (0.6-0.8) would provide more reliable velocities. A higher threshold value excludes more pixels, but the ones that remain are more accurate. In this case, an eventual later interpolation would fill wider gaps of no data. On the other hand, a lower threshold means that more pixels that have a less distinct peak are kept, allowing for fewer data gaps. However, if further smoothing is applied, these data might potentially lead to a slightly biased map.

A second order of postprocessing is employed by using a median filter. A median filter consists of a moving window that substitutes the pixels value at the center of the window (n $\times$ n) with the median of all pixels comprised in the window. Here a 3 $\times$ 3 window has been chosen. Bigger windows allow for filling more data gaps and make the map more complete. However, the filled pixels are not actual measurements but arbitrary interpolations. At the same time, glacier flow is a rather smooth flow and an interpolation of few tens of meters is not unrealistic. For this reason, a kernel size of 30 $\times$ 30 meters seems a good compromise.

The obtained displacement maps for the entire scene ("image matching area" square in Figure 3.1) are then masked for the glacier areas (the actual movement of interest) manually delineated in QGIS. The glacier mask is what has been used to display velocities (e.g. Figure 5.1).

The resulting displacements are then easily converted into average velocities simply by dividing the total displacement by the number of days between the two pairs, in order to get a md^{-1} speed. The final spatial resolution of the velocity maps is equal to 50m.

In order to have a better view of the surface velocity evolution through time for each glacier, two longitudinal center lines have been positioned on both glaciers (Figure 3.1). The extracted velocities have been plotted in a Hovmöller diagram.

4.6 Accuracy of displacements

To evaluate the accuracy of each displacement map, two methods have been used. The first one consists of computing the displacement over some selected stable ground areas for each pair in order to get an overview of the whole matching bias. Secondly, given the absence of ground validation data, a triangulation technique is employed in order to validate the displacements, introduced by Kääb et al. (2016). The assumption behind

the technique is that the sum of the displacement between two subsequent pairs minus the displacement between the first and third image must equal zero (Kääb et al. 2016) following the formula:

$$\overrightarrow{\epsilon} = \overrightarrow{d}_{12} + \overrightarrow{d}_{23} - \overrightarrow{d}_{13} \tag{4.2}$$

where $\overrightarrow{d}$ refers to the horizontal displacements between time 1 and 2, 2 and 3, and 1 and 3, respectively. Therefore, larger residuals indicate less performative triangles, however not giving information on which pair causes high residuals. In addition, it might also be that eventual errors in orthoprojection or other biases are canceled out by the triangulation, also referred to as destructive interference (Kääb et al. 2016). For these reasons, the combination of the two methods gives a solid accuracy assessment method when ground data is unavailable. An occurrence that is very common in such harsh situations, where crevasses derived by high dynamism hinder accessibility.

Chapter 5

Results

A total of 33 flow field maps have been produced. Three examples of the obtained speed maps are shown here:

- $27^{th} August$ 2021 - $11^{th} September$ 2021 (Figure 5.1);
- $23^{rd} June$ 2020 - $02^{nd} August$ 2020 (Figure 5.2);
- $25^{th} May$ 2017 - $29^{th} July$ 2017 (Figure 5.9)

The two glaciers will be analyzed in different subsections, and differences and analogies will be pointed out. For each glacier, three main topics will be covered: flow field on selected image pairs, centerline and cross-transect velocities, and calving front fluctuations.

Note that all dates indicated in the following figures refer to the first date of each pair. For this reason, the very last date of the timeseries and the last two for the triangulation are not presented.

5.1 Kronebreen

5.1.1 Flow field

Kronebreen shows a strong spatial variation of the flow field, regardless of the pair taken into account. Higher velocities are always found around the first 3-4 km from the calving front. The maximum differences reach up to 4 md^{-1}. The higher velocity area is not geometrically at the center of the glacier cross-section, but is centered around the southern part. In-depth insights into this are in the following subsection. Around 3.5 km

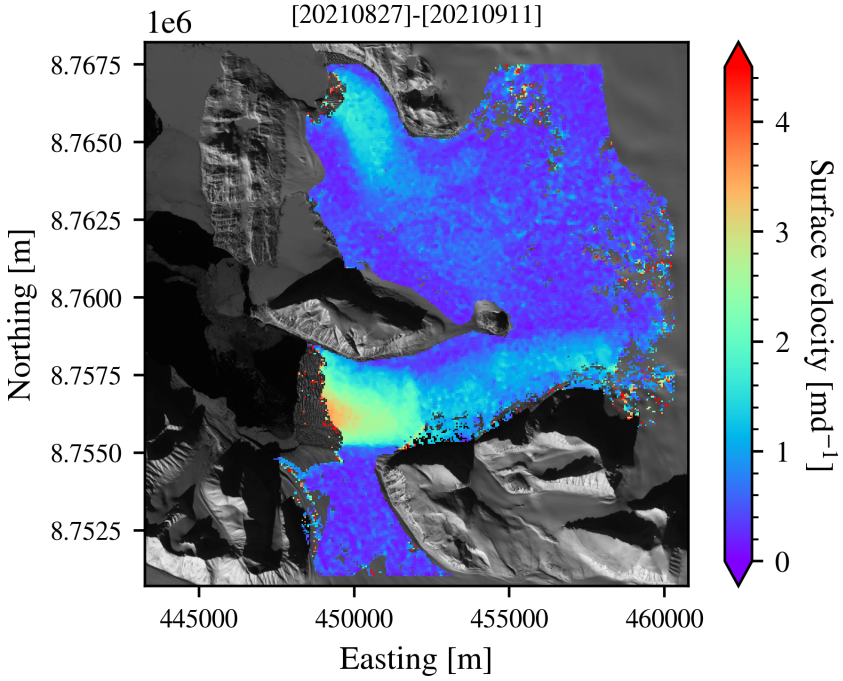

Figure 5.1: Average flow field of Kronebreen and Kongsbreen between 27 August and 11 September 2021. The background image is from 15 April 2017.

upstream of the calving front, a considerable step in velocity is measured (Figure 5.2), where velocity drops of over 1 md^{-1}. Further two steps are less clear but present further upglacier, evident in an aerial photo in Figure 6.4. Apart from the two topographic steps, going upglacier, no clear patterns are found in the velocity field, which appears rather homogeneous. The glacier keeps a constant velocity upglacier both in spring and summer. A strong difference in the velocities is found at the limit towards Kongsvegen (towards South) and at the ice divide to the Kongsbreen catchment. Lateral drag is also evident at the Northern flank of the glacier.

Kronebreen also shows a clear seasonality during the study period. 2019 shows the clearest speedup from spring to summer (Figure 5.3), with high velocities propagating upwards from the calving front. In 2021, the slowdown in late summer (around August) is also well captured by the available images (Figure 5.4).

The highest measured velocities during the study period were recorded in the beginning of July 2019, with velocities of over 8 md^{-1}. In 2017, the pair 25 May - 29 July resulted in the highest speeds with maxima of about 4.8 md^{-1}, whereas 2018 showed a peak just above 5 md^{-1} between 25 April - 8 August. In the last two years of the study period,

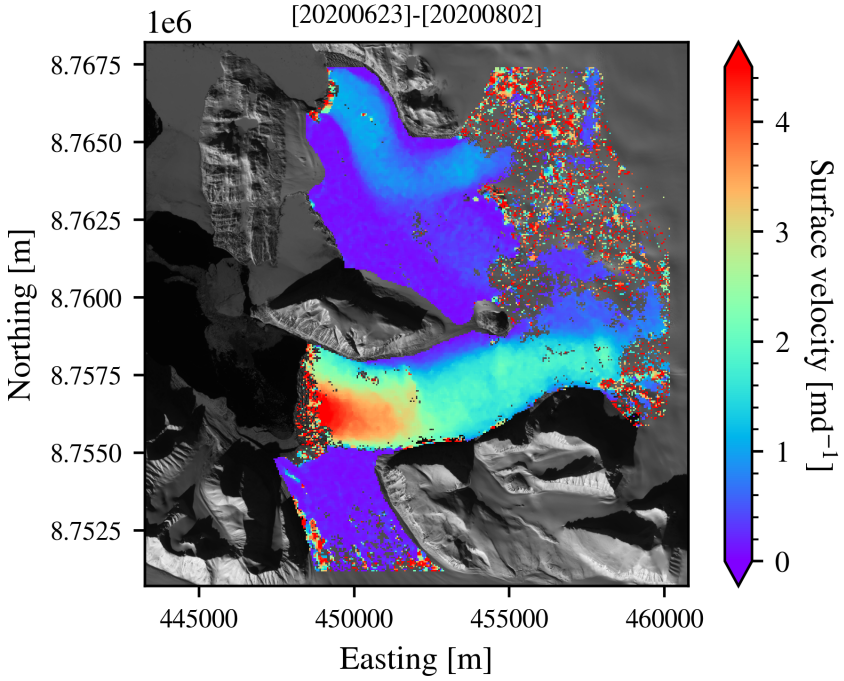

Figure 5.2: Average flow field of Kronebreen and Kongsbreen between 23 June and 2 August 2020. Background image is from 15 April 2017.

maxima of 4.7 md^{-1} and 5.5 md^{-1} were recorded respectively on 23 June - 2 August 2020 and 28 June - 2 August 2021. In all cases in which higher velocities were measured, the average speed of the frontal area (until the drop at 3.5 km from the front) has been the fastest in each year.

Table 5.1: Mean and standard deviation (calculated in time) for three selected points on both glaciers (locations in Figure 3.1). In parenthesis, the amount of Nans found at the point through the whole 33 speed measurements are reported.

	Kronebreen	Kongsvegen
Mean speed front point	3.52 ± 0.72 (nan = 1)	1.47 ± 0.66 (nan = 0)
Mean speed mid point	2.19 ± 0.87 (nan = 3)	1.20 ± 0.68 (nan = 3)
Mean speed up point	1.52 ± 0.75 (nan = 2)	0.81 ± 0.36 (nan = 0)

On the other hand, the lowest velocities are always recorded upglacier, starting from 4-5 km from the calving front. Values are between 1 to 2 md^{-1}, rarely exceeding 2.5 md^{-1}. In some rare occasions (three times) velocities upglacier fall outside these boundaries (e.g.

5 May 2019, 4 July 2019, and 2 August 2020). Those images are affected by coregistration errors which will be discussed later on.

Average velocities through time have been computed on three points on the glacier: one towards the calving front, one above the velocity drop midglacier, and one towards the accumulation basin (Table 5.1). Their locations can be seen in Figure 3.1.

Average velocities throughout the study period show strong variability. As expected, the velocity at the glacier front is much higher than elsewhere, being more than double the one upglacier. The standard deviation is similar for the front and upglacier points, whereas it increases for the midglacier point. However, they weigh differently relative to the average velocity, equivalent to 20.45% (front), 39.72% (mid), and 49.34% (up), respectively.

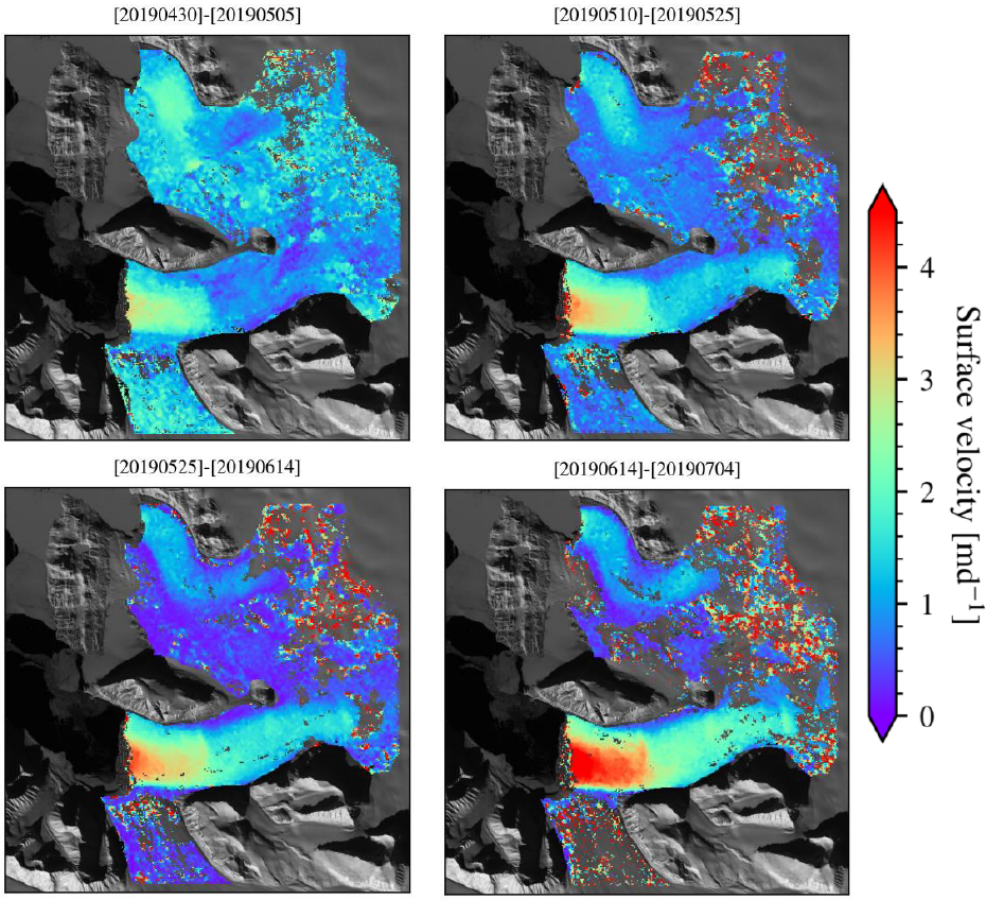

Figure 5.3: Chosen pairs in 2019 showing glaciers seasonal increase in surface velocity from spring to summer

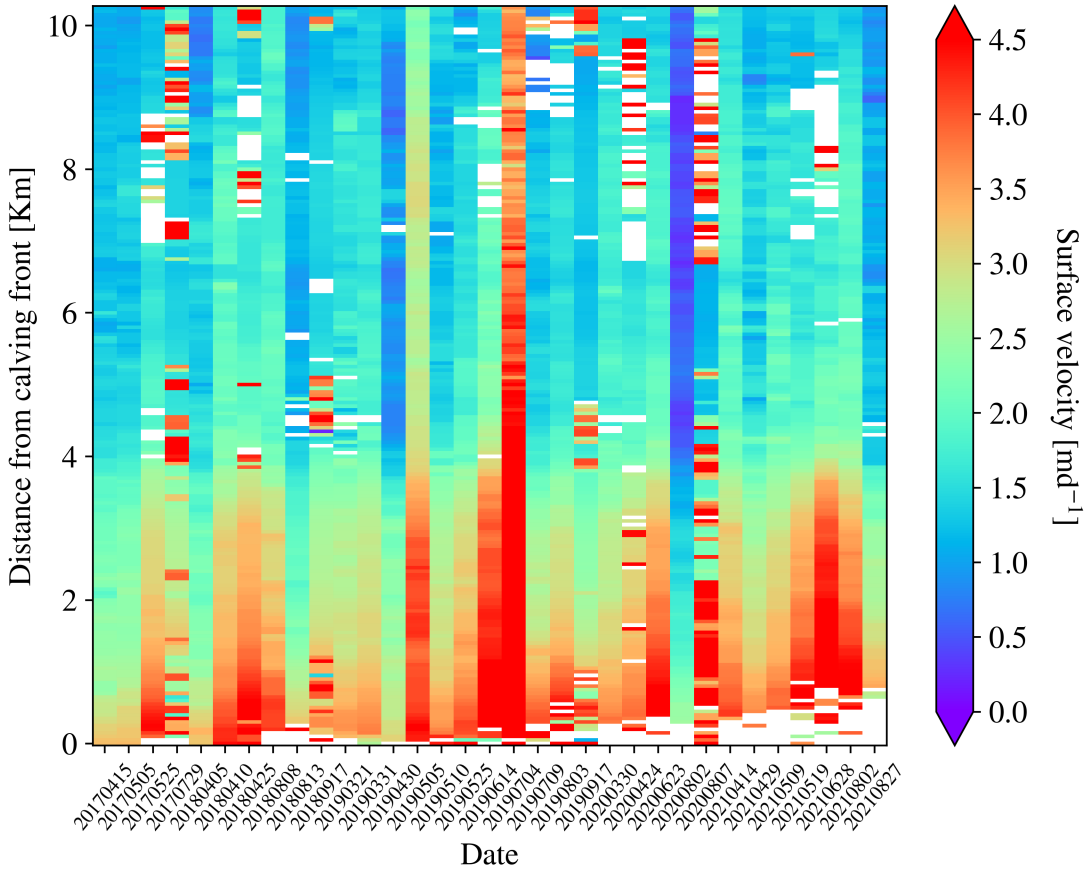

Figure 5.4: Kronebreen velocities timeseries along the centerline. Columns are not proportional to the time difference between dates. White indicates data gaps.

5.1.2 Centerline velocity and cross transect

Figure 5.4 shows the centerline timeseries for Kronebreen for all selected images. All columns are of the same width in order to visualize the centerline velocities of each pair. A second version of the same figure is also plotted (Figure 5.5), in which column width is proportional to the time difference between scenes used to estimate velocities. Recall that dates indicated the start of the pair (i.e. '20170415' refers to the surface velocity measured between 15 April and the following 5 May 2017 scene). The velocity drop of around 3.5 - 4 km from the calving front is apparent also in this case, as in the velocity maps, as well as the seasonality. However, speed changes are enhanced here. Clear outliers and mismatches are clustered mainly above 7 km from the front and at the front, in particular starting from the late 2019 Summer season and until the end of the study period. Outlier pairs are also pointed out in this graph, specifically the ones on 5 May and 4 July 2019, and 2 August 2020. These three pairs will be discussed especially in the

following chapter, as they are affected by coregistration errors.

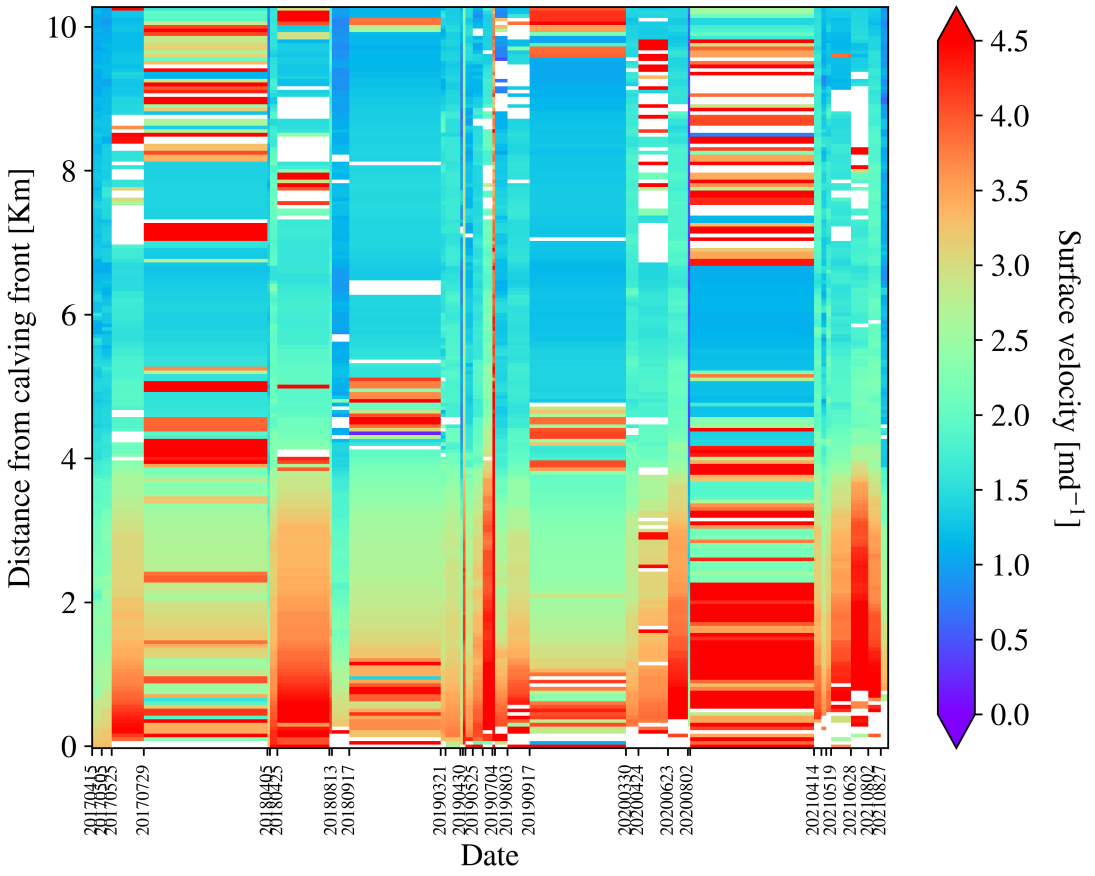

Figure 5.5: Kronebreen velocities timeseries along the centerline. Columns are proportional to the time difference between dates. White indicates data gaps.

All extracted cross-transect velocities on Kronebreen are plotted in Figure 5.6. The transect covers the entire cross-section of Kronebreen of almost 3 km, placed around 2-2.5 km from the calving front. Velocities appear noisy in two distinct portions: in the first kilometer from the northern flank of the glacier, and in the last 500m before the boundary to Kongsvegen. Most of the values amount between 2 and 4 md^{-1}. The velocity curve shape indicates that peak velocities do not occur at the center of the section, but rather on the southern side (left side of the glacier looking downstream), towards Kongsvegen. This pattern occurs in every pair considered. The amplitude between flanks and peak velocity reaches 4 md^{-1}. No clear trends in cross-transect velocities are found.

In order to get an overview of the variability during a single season, velocities in 2019 have been isolated and plotted in Figure 5.7. The reason for this choice is dictated by the amount of available "cloud-free" images. Speedups are not linear along the cross-transect.

In March and April, velocities have similar values (first three pairs). A first speedup occurs at the beginning of May, with a peak increase of about 60% covering the whole cross-section. After a slowdown, a second speedup is recorded in mid-June and July. This time, peak velocities face a three-fold increase reaching 6.5md^{-1}. At the end of the season, the profile assumes the same values as for March and April.

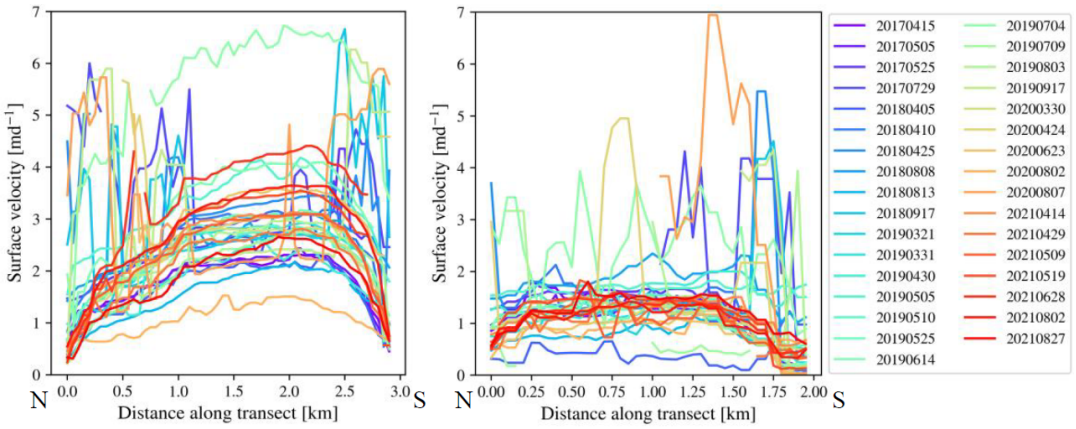

Figure 5.6: Cross transect velocities for Kronebreen (left panel) and Kongsbreen (right panel) during the whole study period

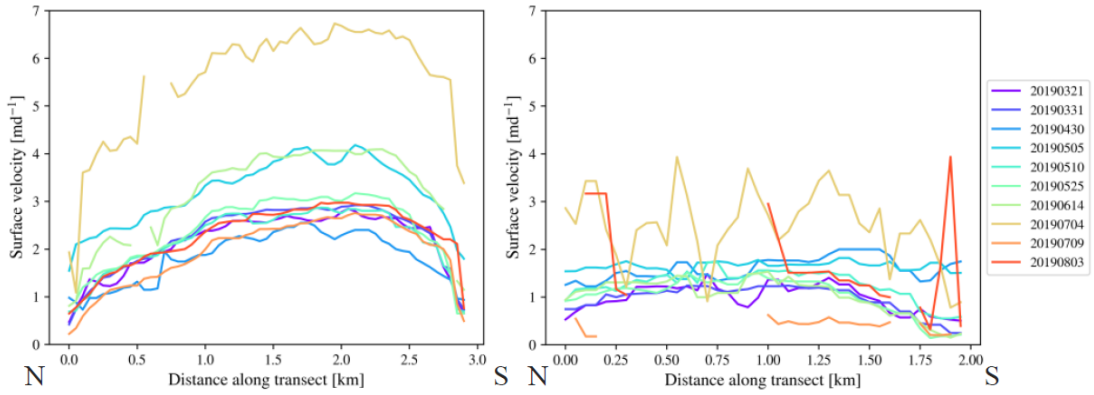

Figure 5.7: Cross transect velocities for Kronebreen (left panel) and Kongsbreen (right panel) during 2019.

5.1.3 Calving front fluctuation

Throughout the study period, the calving front of Kronebreen and Kongsvegen fluctuated notably and faced a strong retreat (Figure 5.8). The front retreat is heterogeneous, ranging from 640 m up to 1.3 km, equal to rates of 128 and 260 myr^{-1}. The highest retreat in the Kronebreen section (1.3 km) has been measured where velocities are the highest (Figure 5.6). A total area of 3.746 km^2 has been lost, corresponding to a loss

rate of 0.75 km^2yr^{-1}.

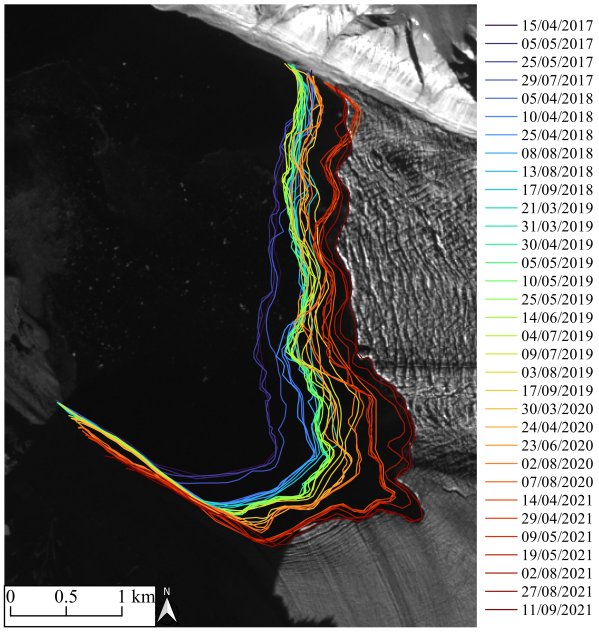

Figure 5.8: Calving front fluctuations of Kronebreen throughout the study period. The base image is from 11 September 2021.

5.2 Kongsbreen

5.2.1 Flow field

Kongsbreen shows a different behavior than Kronebreen both in the velocities and in the spatial variation. The northern part of Kongsbreen is active, whereas the southern one appears almost immobile throughout the whole study period. Peak velocities reach 3 md^{-1} and go barely above this value. These maximum speeds are always found at the front. Velocities are mainly distributed between 0.5 to 2 md^{-1}. Above it, they decline linearly upglacier without steps as found in Kronebreen. Seasonality is also less pronounced. During speedups, the whole tongue increases its velocity almost at the same rate for its entirety. Timings for speedups follow mainly the ones already explained for the other glacier.

Regarding the average velocity at the three selected points on the glacier (Table 5.1), a similar pattern to Kronebreen is found, with higher velocities at the front, decreasing upglacier. However, in this case the decline is rather linear. Standard deviations are consistently lower than for Kronebreen in absolute values. At the same time, their

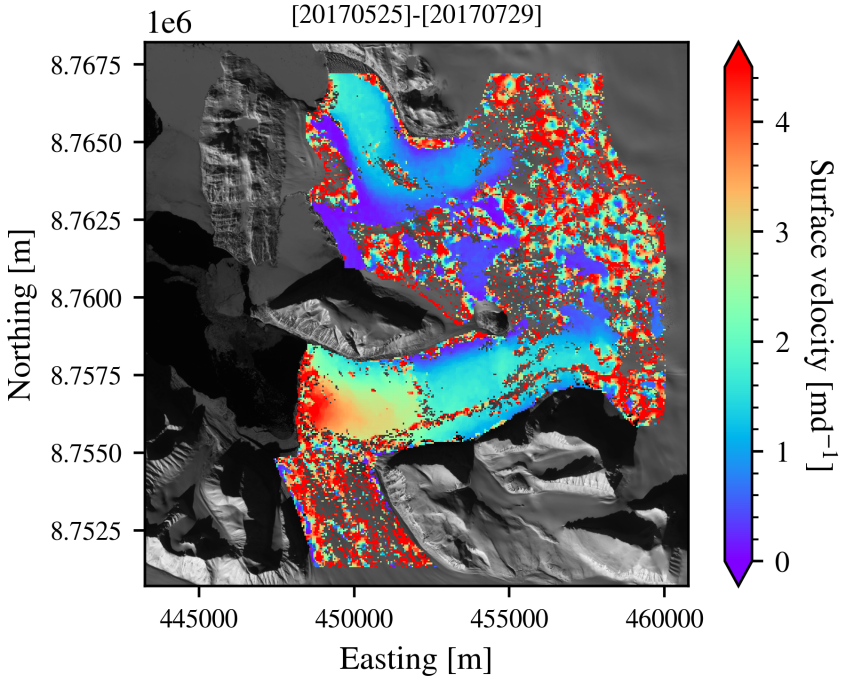

Figure 5.9: Average flow field of Kronebreen and Kongsbreen between 25 May and 29 July 2017

relative weight equals 45% (front), 56% (mid), 44% (up), showing a sharply higher relative deviation.

5.2.2 Centerline velocity and cross transect

The Hovmöller diagram for Kongsbreen is displayed in Figure 5.11, whereas the time difference proportional version of the same plot is displayed in Figure 5.12. The first aspect that the graph highlights is a less pronounced seasonality and an overall lower speed. Higher velocities are found in the first 2 km, except for the 2019 season in which they propagate further upglacier. Missing values and outliers are in this case not concentrated upglacier but rather in a central section between 2 - 5 km from the calving front. The second and third to last missing sections are due to the presence of clouds on the 2 August 2021 image which has been considered nevertheless since Kronebreen and other parts of Kongsbreen were still cloud-free.

Figure 5.6 shows all the measured velocities for the cross-transect on Kongsbreen. The glacier speed mainly remains around 0.5 to 2 md^{-1}, with a lower amplitude than Kronebreen. Outliers are mainly concentrated on the southern part of the transect (right side of the plot). A step is found at 1.75 km, which corresponds to the limit with

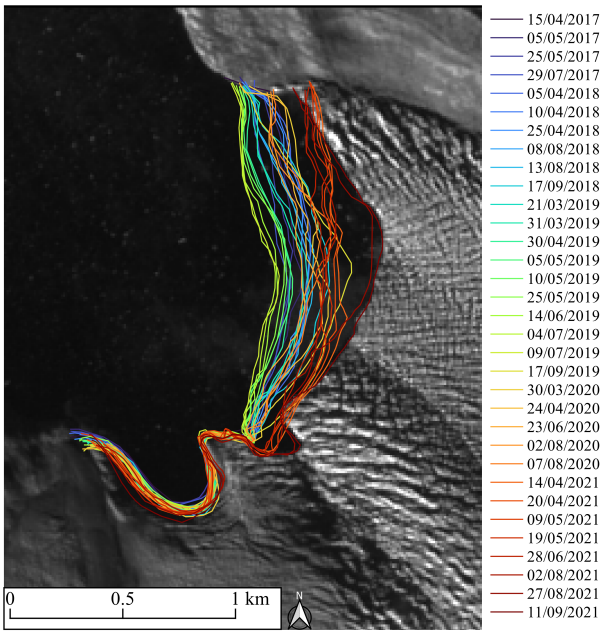

Figure 5.10: Calving front fluctuations of Kongsbreen throughout the study period. Base image is from 11 September 2021.

Kongsbreen South. Apart from this area, Kongsbreen displays a more uniform speed distribution around the center of the cross-section than Kronebreen, which has rather higher velocities in the southern portion. There is no distinct point in which peaks are found, rather a plateau in the 0.5 - 1.5 km interval. No clear trend of velocities during the study period is found.

Taking into account only the 2019 season (Figure 5.7), different speedups are found in late April and July. Regarding the horizontal speed distribution, the whole section shows a uniform higher velocity during speedups on 30 April and 5 May pairs, whereas other pairs show a slowdown for the last 500m of the section, towards the South. The 4 July seems to have a similar behavior but it is too noisy to address it correctly.

5.2.3 Calving front fluctuation

The evolution of Kongsbreen calving front shows a clear retreat during the 5 years study period (Figure 5.10). The change in magnitude is however different from Kronebreen. The maximum measured retreat is around 570m, resulting in an average retreat rate of 114 myr^{-1}. A total area of 0.436 km^2 has been lost, corresponding to an average loss of 0.087 km^{2}yr^{-1} (87'000 m^{2}yr^{-1}). The retreat has however not been linear. The set of fronts in 2019 is advanced compared to the ones in 2017 and 2018. It then migrates

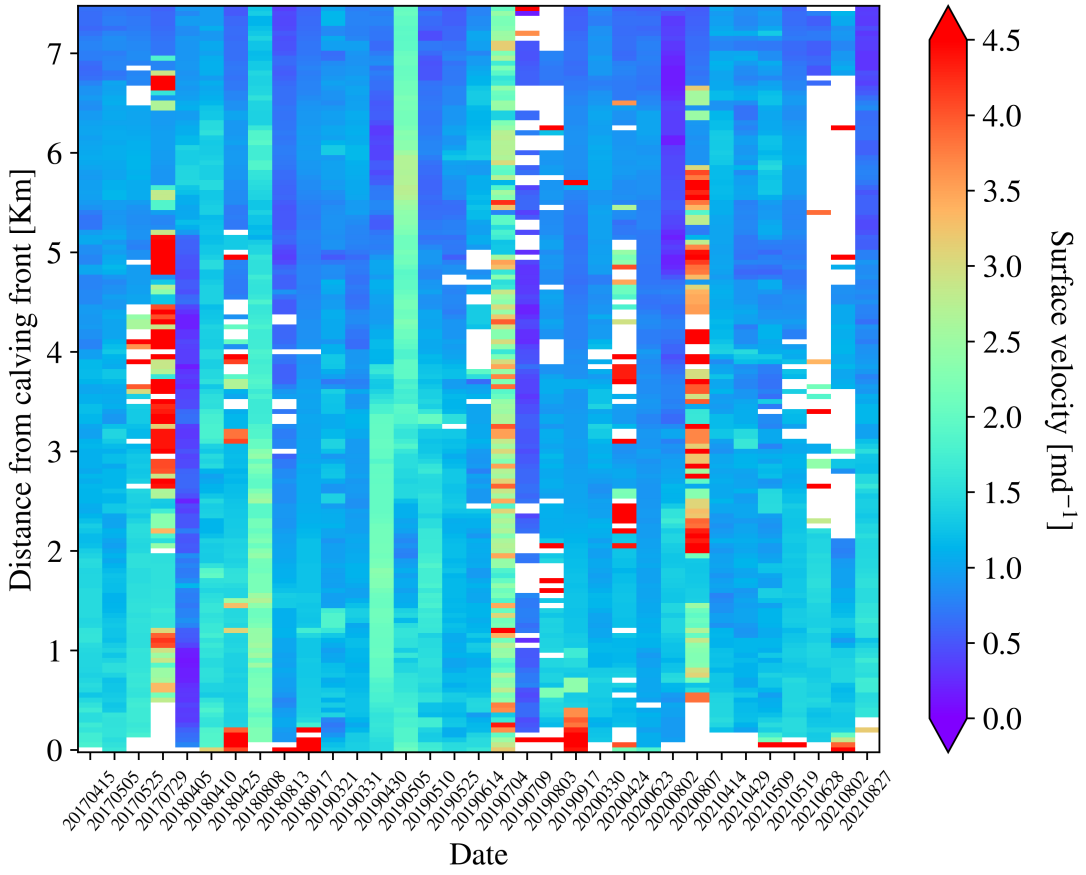

Figure 5.11: Kongsbreen velocities timeseries along the centerline. Columns are not proportional to the time difference between dates. White indicates data gaps.

toward the East at the beginning of 2020 and significant shifts are then recorded by the end of the 2021 season. The amplitude of front differences is notably divided into two parts. On the South, the front remains stagnant for the full 5 years, whereas the changes described interest the upper portion of Kongsbreen.

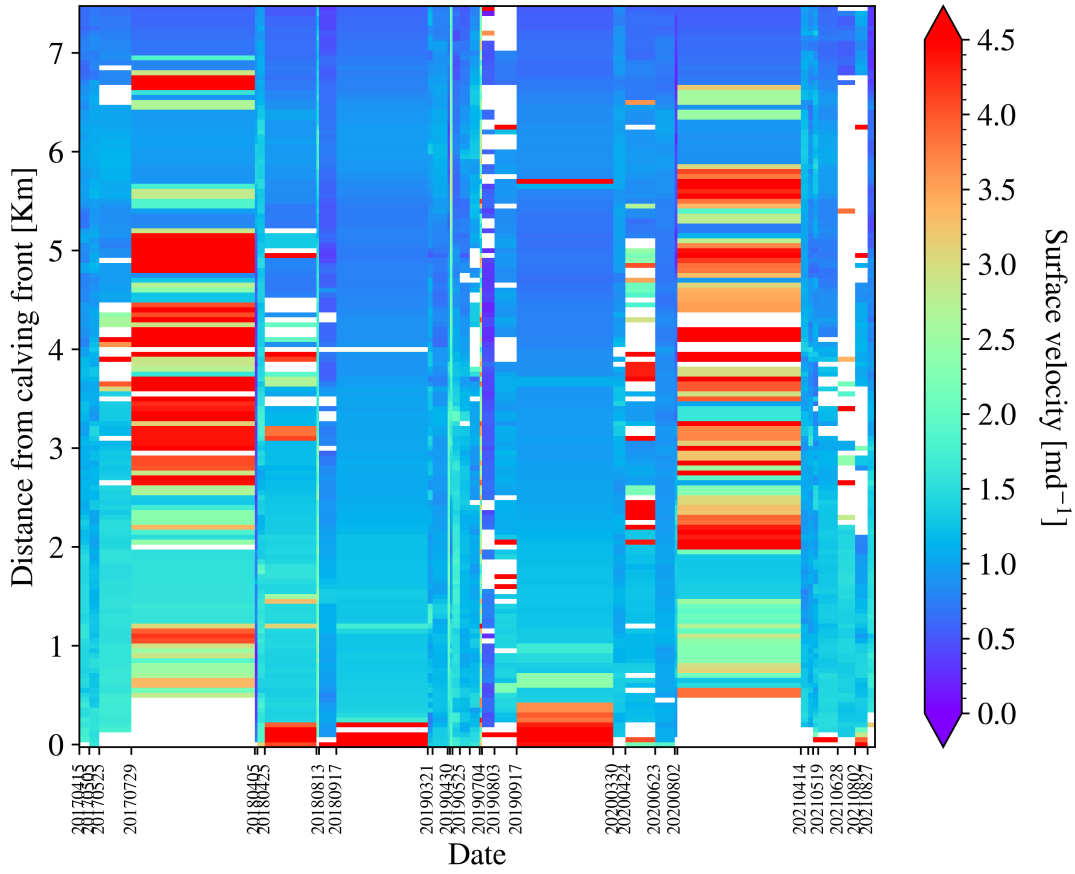

Figure 5.12: Kongsbreen velocities timeseries along the centerline. Columns are proportional to the time difference between dates. White indicates data gaps.

Chapter 6

Discussion

6.1 Accuracy performance

The image matching performance has been evaluated in two ways: i) by computing the displacement over stable ground, ii) by applying the triangulation method described in Section 4.6.

6.1.1 Stable ground

Stable ground displacements are shown in Figure 6.1. The panel on the top enhances unusually high displacements for bedrock, which in theory has to have a movement equal to zero. These pairs have been analyzed one by one, and several reasons arise in considering the high displacements for stable ground.

The most common reason is the snow cover change. Snow pixels have low contrasts and are similar to each other, therefore it is easy that the algorithm finds the apparently same feature in a distant location with a high correlation, resulting in a displacement that is difficult to filter out. This issue has been found in all high displacement pairs (i.e. long time difference between them). Some of them also have clouds scattered over the stable ground area. These images have not been filtered out in the study since the rest of the scene is cloud-free, which still provides valuable displacement data, even though without reliable validation over stable ground. For images late in the season, shadows have covered some stable ground areas, due to longer shadows drawn from mountain ranges. Finally, some of the images are the latest in the season, meaning that the following scene

is from the following year, with early Spring snow cover. In order to capture the glacier movement throughout winter (in which optical images are not available due to the Polar Night), the search area of the matching algorithm had to be increased. As the search area increases, and the probability to find false matches in the scene increases as well.

The lower panel of Figure 6.1 shows the same data but zoomed to the < 20m median displacement which is 25 out of 33 computed displacements. At the same time, a stable ground displacement of e.g. 10m in a 5 days time difference pair has a way higher impact than the same displacement uncertainty for a 25 days-interval pair. For this and other case-specific reasons (clouds, coregistration errors, shadows), stable ground displacements cannot be the only accuracy assessment method for glacier surface speed. Overall, a median ground displacement of less than 15m (for 24 pairs), corresponding to 1.5 pixels, is considered satisfactory.

6.1.2 Triangulation of pairwise matches

A complementary accuracy assessment has been performed via the "triangulation" method as described in Kääb et al. (2016) and displayed in Figure 6.2. The first panel highlights the triangulation results which are notably departing from 0, which should be the expected result of the triangulation. In every case in which the quartile spreads considerably from the zero-line, winter pairs are included in the triangulation. It is a well-known issue that snow cover changes affect considerably optical matching (Heid and Kääb 2012; Huang and Li 2011; Kääb et al. 2016; Van Wyk de Vries and Wickert 2021). The second panel shows the performance of triangulation at a closer scale. All median values lie below the $\pm$10m threshold, which can be considered as a satisfactory result. On the other hand, the spread of quartiles lies outside the 20m (2 pixels) residual in 10 pairs, corresponding to 31% of the calculated triangulation residuals.

The greatest advantage of triangulation is that it provides a validation method when ground data is not available, and rather for the glacier displacements. This work proves that it is possible, to a certain degree, to apply the method in a remote area where ground truth is often logistically complicated to obtain. This method can therefore be used for many other glaciers located in such areas.

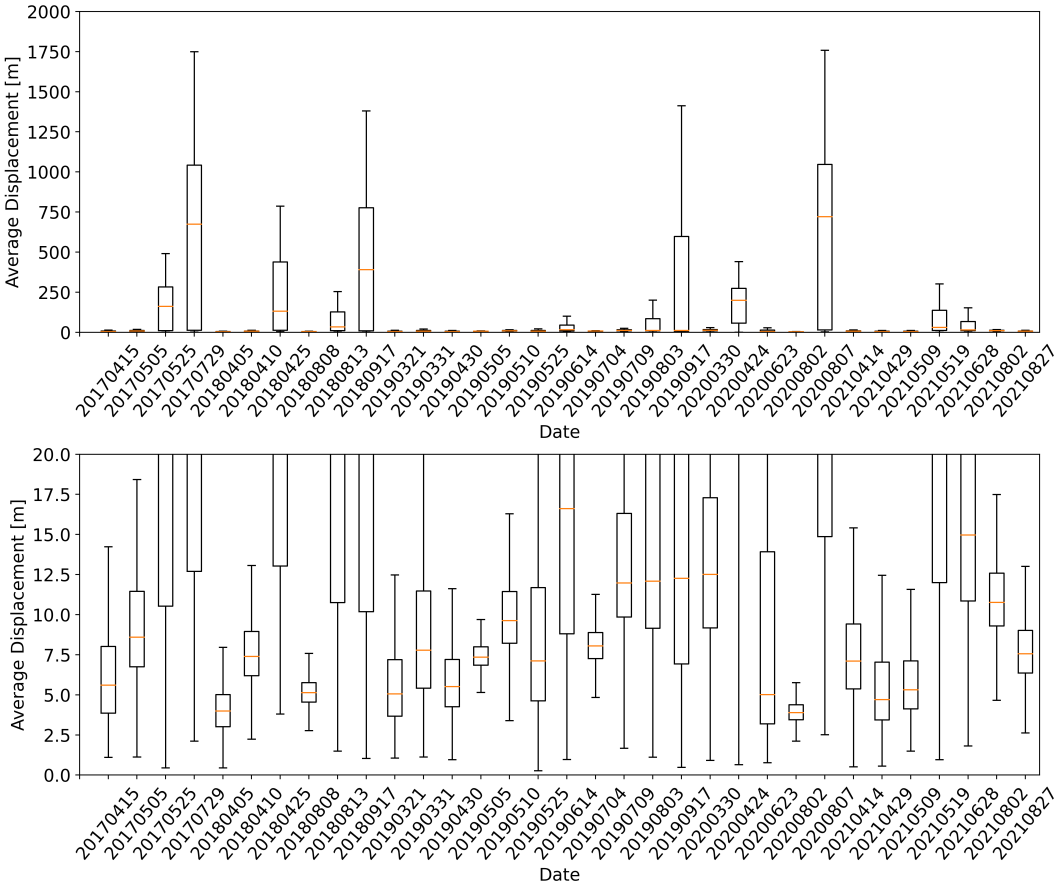

Figure 6.1: Stable ground displacements boxplot for each pair. The upper panel comprises all the values, whereas the lower panel shows the same data but zoomed (note the two y-axis limits). The horizontal orange line indicates the median, boxes extend to the first and third quartiles, and brackets identify max and min.

6.2 Glacier velocities, front fluctuations and comparison with previous studies

6.2.1 Kronebreen

Kronebreen velocities reveal a highly dynamic and active glacier, way more than Kongsbreen. The first clear difference is the glacier geometry. Kronebreen flows almost straight from the feeding catchment whereas Kongsbreen is characterized by a double turn and a stagnant part of the glacier. The measured velocities confirm a strong seasonal variability also found in previous papers. Schellenberger et al. (2015) provides a list of previous studies on Kronebreen, to which Vallot et al. (2017) has to be added. All studies support the idea that there is a strong control between the water input into the

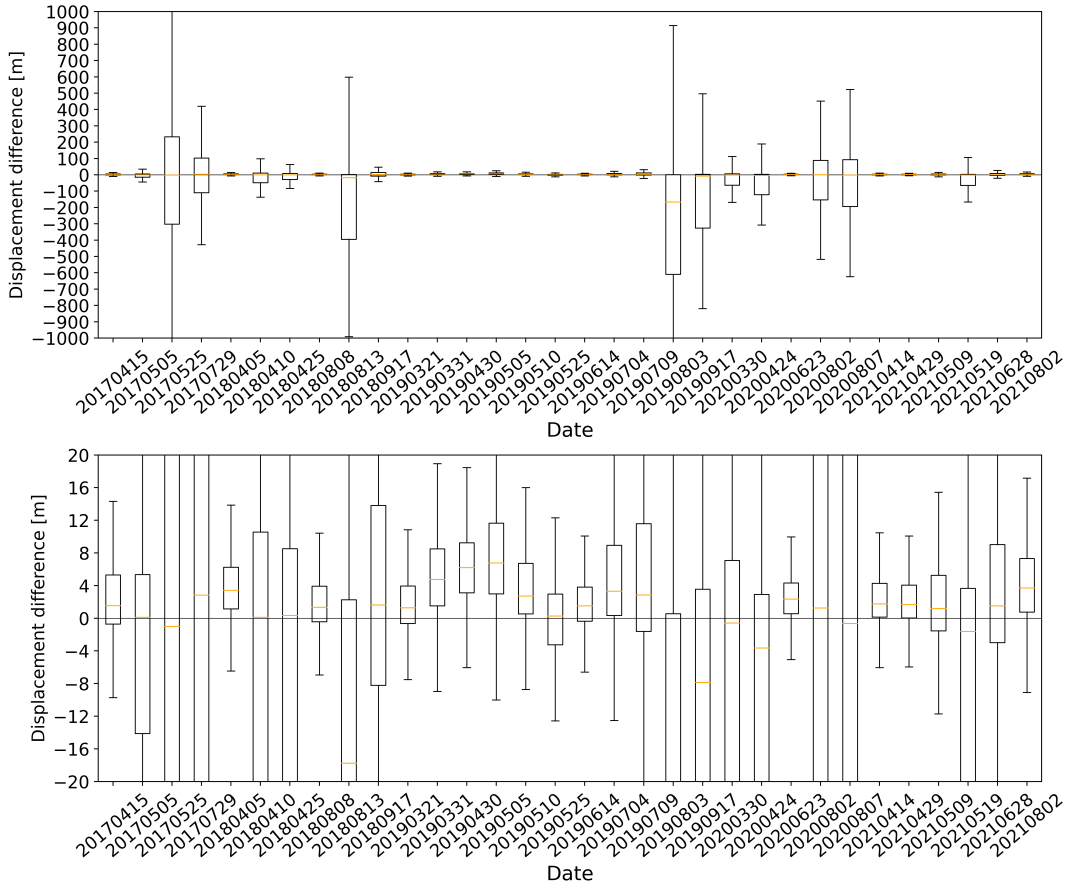

Figure 6.2: Triangulation results for each pair. The date identifies the first of the triangulation calculation (t1). Data in both panels is the same, upper panel has a larger y-axis to include all values. The lower panel shows closely the spreading around 0.

subglacial system and the velocity. As explained in the Introduction, ineffective drainage systems are able to hold water at the glacier base. With further water input, lubrication and water effective pressure increase enhances glacier sliding and accelerates it in spring and summer.

The main finding on Kronebreen speed fields is that the glacier is accelerating. Kääb (2005b) measured front velocities up to 2md^{-1} in the early 2000s, Köhler et al. (2012) found peaks around 3md^{-1} in 2009 and 2010, Schellenberger et al. (2015) registered 3.2md^{-1} in 2013, whereas this study, registered peak velocities are above 5md^{-1}. Nevertheless, the calving front is substantially retreating. This means that the rate of calving overcomes by far the advancement due to speed increase. The long-term trends for Kronebreen have to be considered in connection to the possibly upcoming surge of the neighboring Kongsvegen (Bouchayer et al. 2023). Their common front point retreated by

1.2 km in the study period (5 years), at a rate of 240m per year. Having kept the same rate (or even slightly higher), the fronts are nowadays separated.

The relationship between the velocity at the front and the front change is displayed in Figure 6.3. 2019 is the most complete year in terms of velocity measurements and a seasonality is evident. In March, the glacier advances by 3 meters per day, when water and air temperature are still low. As the season goes on, the velocity increases and keeps the front stagnant as seen on 14 June and 4 July. As the velocity decreases, the front faces an abrupt retreat on 9 July and 3 August, despite velocities of 3.4 and 3.8 md^{-1} respectively. Overall, peaks in advancement (or stagnation) are seen mainly at the beginning of the season, whereas retreats are always late. An exception is the 19 May 2021. A comprehensive analysis is however not possible given the lack of data on precipitation, melt, air, and water temperature, which are all factors that strongly influence the calving rate and flow speed. In addition, the plot shows an overall trend of increasing velocities for Kronebreen, as well as considerably higher velocities for front movement compared to previous studies as reported in the previous paragraph.

The peak at 7 md^{-1} on 4 July 2019 is affected by a strong bias due to coregistration error (Figure 6.1. Both stable ground and triangulation results on this date might seem low at first glance. However, given the short time difference, the median stable ground displacement of 8m results in a bias of $1.6md^{-1}$. The triangulation result on this date also indicates a median residual of 3.5 meters. With the triangulation, it is hard to say which of the three pairs used contributes more or less to the error. But given the coregistration error for the 9 July image (with which the pair 4 - 9 July is processed), it is easy to point to it as the main contributor to the error. At the same time, if it is assumed to remove $1.6md^{-1}$ from the $7.2md^{-1}$ peak, it would still result in a considerable velocity peak of $5.6md^{-1}$. To be more precise, the velocity peak might actually be higher than $5.6md^{-1}$ since the coregistration error vector is not fully parallel to the flow movement. Therefore only a part of it should be subtracted from the measured displacement (and consequently from the average velocity). Coregistration errors are also responsible for the high and low velocities on 5 May 2019, 4 July 2019, and 2 August 2020. The reason why coregistration errors create both unusual peaks and drops is that the errors are not uniform from pair to pair. On top of that, the direction of the error affects differently the glaciers' speed in the scene depending on their flow direction. A coregistration error

opposite to the glacier flow will produce a low-biased result and vice versa.

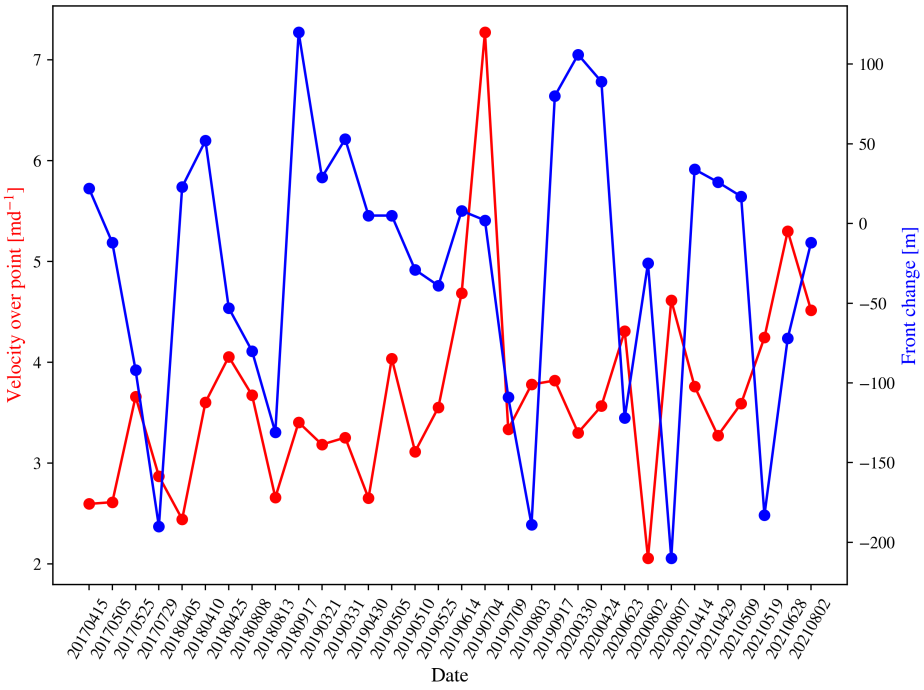

Figure 6.3: Front change measured along the centerline and velocity of the front point of Kronebreen. Positives are advances and negatives are retreats

The Kronebreen increase in velocity with time is also evident in the comparison of centerline velocities and cross transects. Cross transects reveal that the highest velocity is not aligned with the center of the glacier section as in previous studies. The step in speed 3-4 km from the front is analogous as found by Kääb (2005b) and Schellenberger et al. (2015). The position and the magnitude of the step are however different given the increase in velocity that Kronebreen is facing. The reason for the abrupt step has to do with the bedrock topography. As presented in Vallot et al. (2017), there are steps and cross-section troughs in the bedrock, which lead to icefalls on the glacier surface (Figure 6.4) which are visible also in the maps produced here.

6.2.2 Kongsbreen

Kongsbreen has the particularity of the division into two branches. The Northern part has a dynamic behavior, whereas the Southern part is almost stagnant. The reason for this is related to the bedrock topography, that Lindbäck et al. (2018) have mapped using radar transects. The Southern part of the glacier is stagnant since it is sitting on

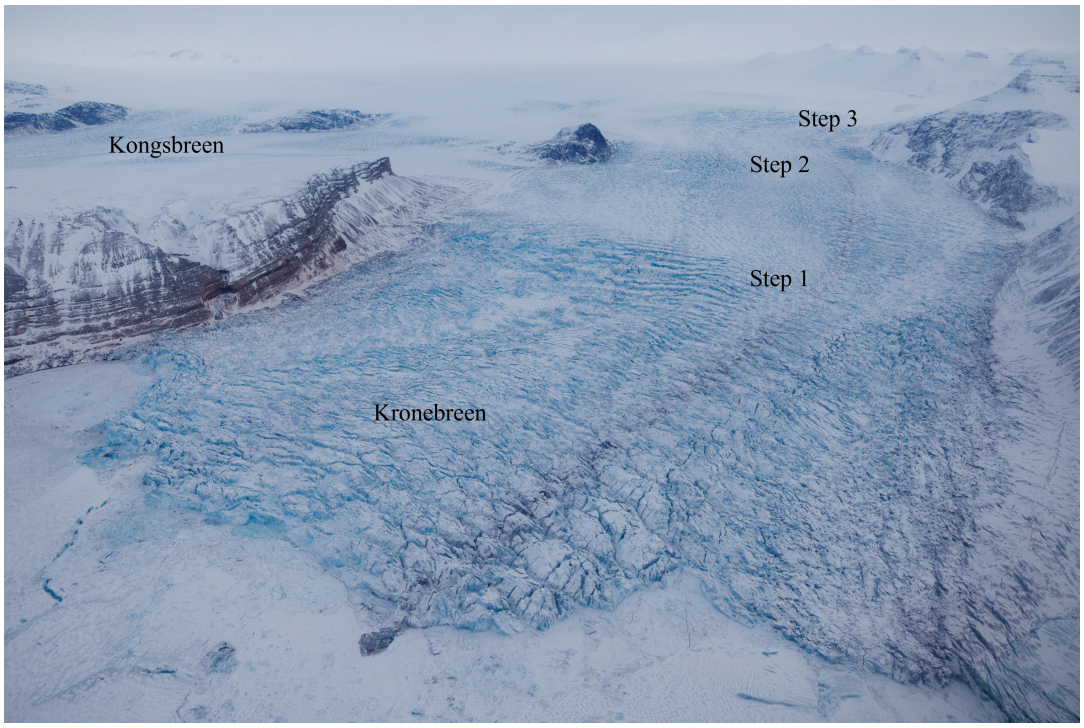

Figure 6.4: Studied part of Kronebreen as seen from an aerial view. The picture has been taken on the 5th of April 2023. The three steps in velocity are evident, as they are marked by intense crevasses. Photo from Lisi Niesner.

bedrock. Few crevasses are in fact visible due to the lack of dynamism. The glacier is fully grounded, therefore strongly influenced its drainage system. The high velocities found on the northern part are possible only through basal sliding. In fact, as many other glaciers in North-Western Svalbard, temperate basal conditions are present (H. K. Björnsson et al. 1996). Schellenberger et al. (2015) did not find very distinct peaks in summer, and this has been confirmed here (Figures 5.11 and 5.3). They suggested that an inefficient drainage system is present. However, it is hard to compare the reasons for it since they matched speeds with weather data and rain events, which are missing in this work.

The previous work on Kongsbreen is way more limited than for Kronebreen. Studies that analysed Kongsbreen velocities are only two: Schellenberger et al. (2015) and Schild et al. (2018). Schellenberger et al. (2015) computed velocities in 2007 - 2008, and from 2009 continuously until 2013 using a compilation of radar and ground GPS measurements. Comparing their results with the ones of this study, there is no clear trend (speeding up or slowdown) in the glacier velocity. Velocities appear to be very similar over time. The measured peak velocity here is just above 3 md^{-1} whereas they measured 2.7^{-1}. Schild

et al. (2018) used radar as well to compute velocities in 2016 just at the calving front area. Their averages appear slightly lower than the ones in this study for the Kongsbreen point in the front (Table 5.1), even though they used a small area to make their average (Schild et al. (2018) Figure 2b, white box).

Front positions reflect the balance between glacier velocity and calving rate. An advance is usually observed in late spring and early summer when the velocity increases and water temperature is not warm enough to induce undercutting and trigger intense calving (Köhler et al. 2012), as observed for Kronebreen. On the other hand, in late summer, water temperature increases, inducing melt and undercutting, resulting in a front retreat. Luckman et al. (2015) proved that there is a strong relationship between water temperature and frontal ablation rate, especially for Kronebreen ($R^2 = 0.84$).

Figure 6.5 shows the front change together with the front velocity on a chosen point for Kongsbreen. Four retreat peaks are identified (above 50 meters of retreat, i.e. $>$ -50m) in all years except for 2018, where the retreat seems more gradual. Peak retreats occur in July twice (2017 and 2019), in early August once (2020) and in late June once (2021). It is clear that these values are highly influenced by the manual precision in locating the exact front point, uncertainties in the velocities, local heterogeneity, and mainly the scene dates. Images are acquired at specific times, according to the satellite orbit, and they might not necessarily coincide with the glacier's seasonality, peak retreats, or peak velocities, adding a bias to the analysis. The presented analysis is therefore not sufficient to draw conclusions about actual glacier peak velocity throughout the season, for which continuous GPS measurements would be needed (which in turn would not have the spatial scale). However, the graph shows that positive peaks in the front change mainly occur when the point velocities are below 1.5 md^{-1}. This is in fact counter-intuitive with regard to the theory. Data on rain events, air temperature, water temperature, and higher temporal resolution images (or GPS measurements) would therefore be needed for a comprehensive understanding of the trends shown.

6.3 Limitations of the method

In order to discuss the spatial performance and limitations of the algorithm, selected peak correlation maps (Figure 6.6, same dates as the speed maps) and the map of Nan count (Figure 6.7) intended as the sum of times that a specific pixel has been a Nan

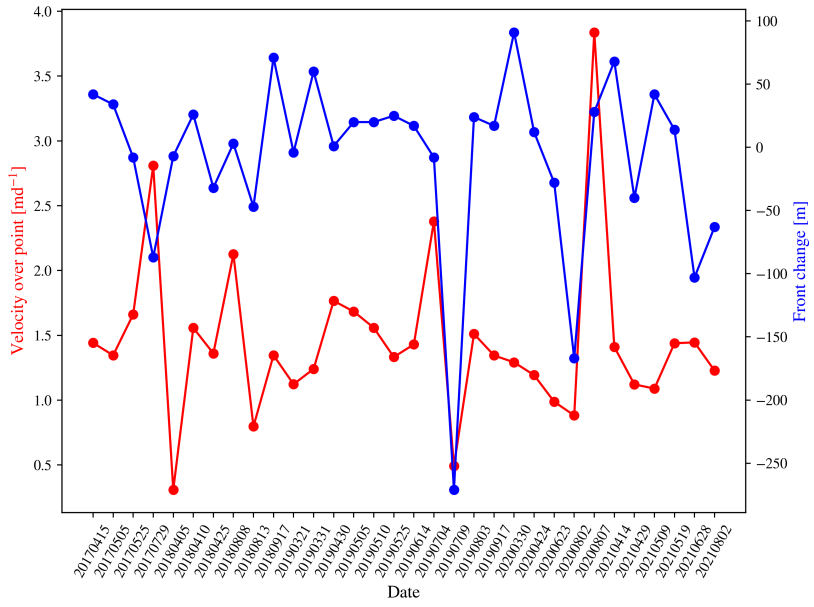

Figure 6.5: Front change measured along the centerline and velocity of the front point of Kongsbreen. Positives are advances and negatives are retreats

(i.e. a non-matched feature), are shown. In Figure 6.6, the performance increases from left to right. The highest concentration of high values is clustered in heavily crevassed areas on both glaciers. This was expected, as crevasses constitute optimal features to be tracked. Nan counts follow as well in these areas, with the highest concentration of a low (in some cases zero) number of Nans. Kronebreen is more dynamic than Kongsbreen and has indeed a greater portion of the glacier with low Nan counts.

On the other hand, low correlation values are concentrated on non-crevassed areas primarily. For instance, Kongsbreen South has non-crevassed patches, which can be identified easily by looking at both peak correlation maps and Nan count. The biggest area with low correlation values and the highest Nan count is concentrated in the glacier accumulation areas. Here, the presence of almost constant snow patches hampers the matching performance. Indeed, snow cover changes are known for being the most common limitation of the presented method (Heid and Kääb 2012; Kääb et al. 2016). Their low visual contrast, the broad similarity between patches, and their highly dynamic nature in spring and summer are the main reasons.

Another limiting factor that arises in the presented figures is the presence of shadows, clearly visible in the third panel (Figure 6.6), on the southern part of Kronebreen. The study area experiences the Polar night where high solar zenith angles are reached. As a

consequence, long shadows cover parts of the glacier which makes it difficult to match.

The disappearance of features between images also brings errors or mismatches. This is evident in the first panel to the left in Figure 6.6 and in the Nan count map (Figure 6.7) as a tiny line with a higher Nan count. The same is visible in the speed map in Figure 5.9. The medial moraine appears and disappears according to glacier ablation. It constitutes a high-contrast feature that is well identified, but not tracked in the following scene.

Finally, from the Nan count map, glacier fronts increasingly have Nans going toward the fjord. The glaciers outline (i.e. glacier mask) has indeed been kept the same throughout the study period. With the ongoing front retreats mapped in Figure 5.8 and Figure 5.10, Nans are obviously generated.

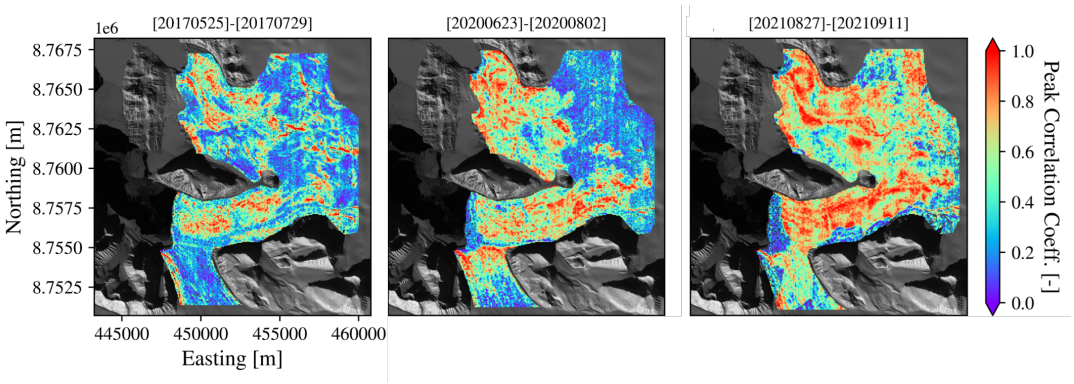

Figure 6.6: Peak correlation maps for three selected pairs

In order to have a sound idea of the uncertainty of the calculated velocities, one has to in parallel look at the stable ground displacements (Figure 6.1) and the triangulation results (Figure 6.2) for each pair. Stable ground displacements are, as the entire scene, affected by snow cover changes. In the Arctic, snow is present for around 9 months per year, whereas in the accumulation area of glaciers almost all-year (Killie et al. 2021). The selected stable ground areas are as much as possible homogeneously flat and far from mountain ranges. These areas are limited, and affected by shadows and/or snow cover changes. This means that a pair with high stable ground displacements might not be necessarily discarded or that glacier velocities are biased in the affected pair. It is however true that there is in this case a lack of "ground truth" to validate data. For this reason, the triangulation method provides a complementary means for validation, which is easy to apply and gives a comprehensive view of potential errors in matchings. On the

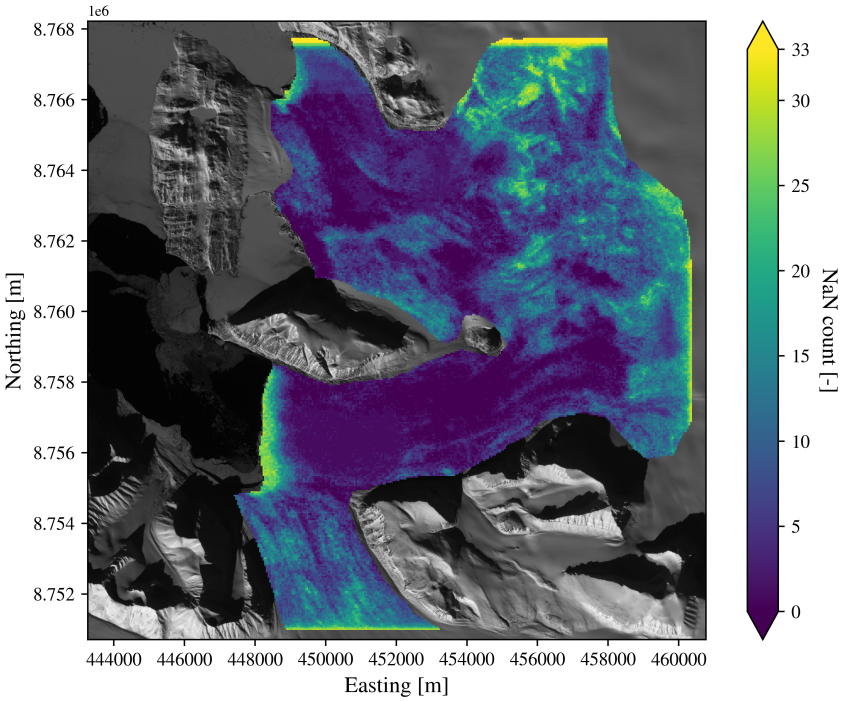

Figure 6.7: NaN count map for all pairs

other hand, this method takes into account three images and three pairs, with a related increase in uncertainty factors.

The ”adaptive search window” method has been introduced to analyze the time series. The method proves to be convenient in the sense that it tries to set the best-fitting search window for each pair. The ”best fitting” is intended to be the search area that manages to capture the highest displacement in the pair. This is of course not easy, given the wide range of displacements that glaciers experience. Ideally one should know the maximum displacement for each pair. The reason for this is that the bigger the search window, the higher the chances that the algorithm matches the wrong features. Simply because when searching for a larger area, features are more, and therefore there are more chances for a match. If one has to match a few images, the adjustment of search areas can be done manually and with some degree of trial and error. For a longer time series, this becomes time-consuming and therefore not applicable. This is why in this work an adaptive search window has been used. In some cases, it worked better than in others. As an example, Figure 5.9 displays a rather low performance of the matching. Having multiplied an average velocity by the time difference between the two pairs, the difference between 25 May and 29 July amounts to 65 days which converts to a search area equal to 78

pixels (780m), according to the proposed methodology. The residuals of the triangulation are in fact rather high (Figure 6.2) and the stable ground displacement as well (Figure 6.1). This was clearly expected, as it has been shown already that the number of outliers increases with the temporal separation between pairs (Nagy et al. 2019).

The choice of the template has been 11x11 (110x100m) following Kääb (2005b). Different templates have an influence on the results for the same scene (Debella-Gilo and Kääb 2012). Bigger template sizes are more prone to be influenced by surface deformation between the images whereas smaller ones might not capture the trackable feature (e.g. a crevasse) (Kääb 2005b). Kääb (2005b) used a threshold of 0.6 for the peak correlations, whereas here 0.5 has been used. The reason for this has been to include most of the data in order to discuss mismatches spatially, sacrificing the reliability of the data. The main parts of the glacier have however peak correlations above 0.6, and also in their work, issues with snow-covered areas have been found.

To sum up the uncertainties, a comparison of the images matched for low-performance pairs is reported in Figure 6.8. All the discussed sources of error or mismatches are included in the selected pair and listed in the figure caption.

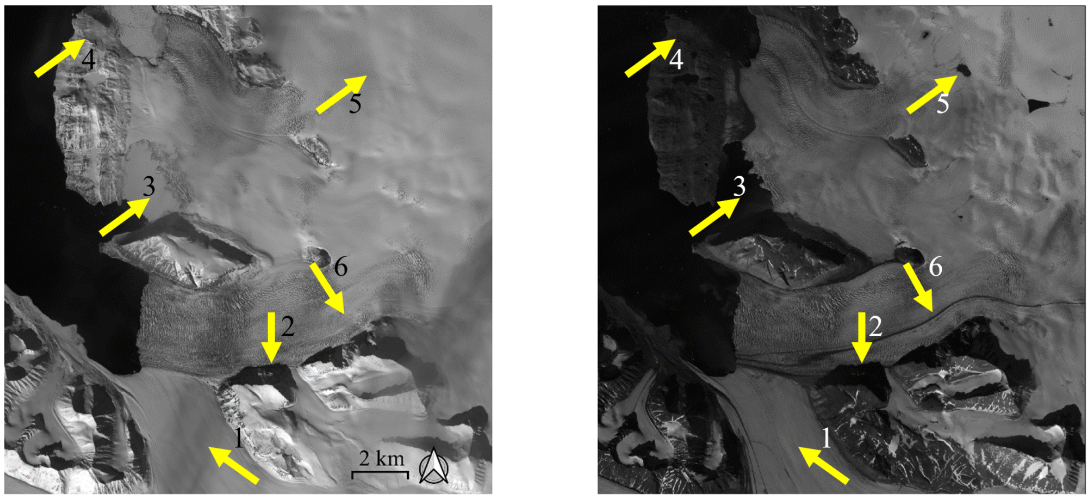

Figure 6.8: 25 May and 29 July 2017 Sentinel-2 L1C images used to compute the velocity. Arrows indicate the source of error in the matching: 1) clouds, 2) shadows, 3) sea ice, 4) snow cover on stable ground, 5) appearing features, 6) disappearing features.

A last source of uncertainty worth mentioning comes from the data itself, for which Kääb et al. (2016) and Nagy et al. (2019) already give a sound overview. Co-registration and orthorectification of the images already introduces errors in the provided images.

These are corrected before product delivery using Digital Elevation Models (DEMs), which should approximate the glacier surface. DEM elevation might not correspond to the glacier elevation and also the time stamp of a DEM often does not match the timing of the Sentinel-2 overpass (Kääb et al. 2016). For highly dynamic and changing glaciers, the errors in orthorectification DEMs result in a considerable source of error. At such high latitudes, the Shuttle Radar Topography Mission (SRTM) did not acquire data. Therefore, the DEM used in such a high latitude zone is the Planet DEM. At the same time, Nagy et al. (2019) reports that the unavailability of Planet DEM 90 makes it complicated to understand how it is used to fill the voids left by SRTM. In addition, as reported by the user guide for Sentinel-2 (https://sentinels.copernicus.eu/), since March 2021 the L1C products are orthorectified using the Copernicus DEM GLO-90m, based on data coming from the TanDEM-X Mission. This means that the last season's data has been corrected with a different DEM. Assessing differences in the orthorectification and its impact on displacements is however not the scope of this work.

Some scenes used in this study are clearly affected by coregistration errors as reported, for which however a correction has not been employed. These errors are affecting pairs differently according to the coregistration error direction, the time difference between the images, and the flow direction of glaciers. In the case of the 4 July 2019 velocity outlier (Figure 5.4), the direction of the coregistration error is the same as the glacier flow. In addition, the time difference with the subsequent image is just 5 days. As a result, the error introduced is considerably high.

Chapter 7

Conclusion and perspectives

The presented work aimed at contributing to the monitoring of surging and fast-flowing glaciers in Svalbard. For Kronebreen in particular, this work adds to the monitoring of a long-studied glacier that has been observed to surge before. In particular, this study constitutes the second multi-annual work on Kronebreen, after Schellenberger et al. (2015). An intra-annual variability up to $4 md^{-1}$ and peak velocities of over $5 md^{-1}$ (e.g. corrected 4 July 2019) have been measured. Inter-annual comparison with previous studies shows that the glacier is accelerating. Seasonal speedups are mainly occurring around June-July, affecting mainly the lowermost 4 km above the calving front. The seasonal acceleration up-glacier is less pronounced than at the front. In addition, the front is receding at a rate of 0.75 $km^2 yr^{-1}$.

Regarding Kongsbreen, this manuscript follows up on the previous work by Schellenberger et al. (2015) in monitoring a fast-flowing glacier in Svalbard. Velocities for the northern part ranged from 0.5 to $2 md^{-1}$, usually declining linearly up-glacier. Speed-up timing followed the ones found for Kronebreen. Acceleration affects the entire glacier at the same rate. On the other end, the southern part of the glacier remained almost stagnant for the whole study period. Comparing the velocities with the only previous study (Schellenberger et al. 2015), there is no trend and values are rather similar. Kongsbreen front is retreating as well, with a rate of 0.087 $km^2 yr^{-1}$ (87'000 $m^2 yr^{-1}$).

Kongsbreen has never been observed to surge, but many glaciers around it did. With the ongoing climate change, it is hard to make predictions. However, Kongsfjorden has been identified as a particularly susceptible area to study climate change impacts (Trusel et al.

2010). The specificity of the site is given by three highly diverse glaciers flowing into the same fjord. One fast-flowing non (yet) surging glacier (Kongsbreen), one fast-flowing surging glacier (Kronebreen), and one stagnant but expected to surge surging glacier (Kongsvegen) (Bouchayer et al. 2022).

This manuscript explored the limitations of applying optical remote sensing to monitor glacier velocities in Svalbard. Some of the sources of uncertainties listed in Figure 6.8 could be improved with the workflow. For instance, cloud masks can be employed to automatically select images instead of manually selecting them, or simply by taking just cloudless data as Kääb et al. (2016) (Section 3.1, second paragraph). Identifying cloud pixels over the glacier masks and applying a threshold on the percentage of cloudy glacier area for discarding images could be an interesting implementation. Accurate coregistration or correction for those errors could further improve the speed maps accuracy obtained here. The matchings could also be improved via preprocessing methods. Edge detection (Ahn and Howat 2011), multi-band exploitation via PCA (Scambos et al. 1992), Wallis operator for contrast enhancement (Gardner et al. 2018), are among the examples. None of these have been employed in this work. Optical remote sensing in such areas has strong limitations as seen throughout the present work, therefore some preprocessing might be beneficial for improving matchings.

Leclercq et al. (2021) analyzed the potential of Sentinel-1 radar data to detect surge activity, given the ability of radar to acquire through clouds, snow, and during the Polar night. For the same reasons, at high latitudes, glacier studies have been mainly performed using radar data. However, the revisit time of Sentinel-1 is 12 days, almost 2.5 times more than the (potential) Sentinel-2 one. Surging glaciers still have many unanswered questions about their probability, distribution, and behavior (Koch et al. 2023). The higher temporal resolution of Sentinel-2 could provide more data to be combined with radar ones in order to fill the gap between radar acquisitions and construct the most continuous possible time-series.

References

Ahn, Y. and Howat, I. M. (2011). 'Efficient Automated Glacier Surface Velocity Measurement From Repeat Images Using Multi-Image/Multichip and Null Exclusion Feature Tracking'. In: *IEEE Transactions on Geoscience and Remote Sensing* 49.8, pp. 2838–2846. DOI: 10.1109/TGRS.2011.2114891.

Barrett, B. E. et al. (2008). 'Distribution and character of water in a surge-type glacier revealed by multifrequency and multipolarization ground-penetrating radar'. In: *Journal of Geophysical Research: Earth Surface* 113.F4. DOI: https://doi.org/10.1029/2007JF000972. eprint: https://agupubs.onlinelibrary.wiley.com/doi/pdf/10.1029/2007JF000972.

Beaud, F. et al. (2022). 'Surge dynamics of Shisper Glacier revealed by time-series correlation of optical satellite images and their utility to substantiate a generalized sliding law'. In: *The Cryosphere* 16.8, pp. 3123–3148.

Benn, D. and Evans, D. (2014). *Glaciers and Glaciation, 2nd edition*. Taylor & Francis.

Benn, D. I. et al. (2019). 'A general theory of glacier surges'. In: *Journal of Glaciology* 65.253, pp. 701–716. DOI: 10.1017/jog.2019.62.

Bergh, S. G., Maher, H. D. and Braathen, A. (2000). 'Tertiary divergent thrust directions from partitioned transpression, Broggerhalvoya, Spitsbergen'. In: *Norsk Geologisk Tidsskrift* 80.2, pp. 63–81. DOI: 10.1080/002919600750042573.

Beszczyńska-Möller, A. et al. (1997). 'Estimation of glacial meltwater discharge into Svalbard coastal waters'. In: *Oceanologia* 39.3, pp. 289–298.

Bhambri, R. et al. (June 2011). 'Glacier changes in the Garhwal Himalaya, India, from 1968 to 2006 based on remote sensing'. In: *Journal of Glaciology* 57, pp. 543–556. DOI: 10.3189/002214311796905604.

Bindschadler, R. et al. (1977). 'Geometry and Dynamics of a Surge-type Glacier'. In: *Journal of Glaciology* 18.79, pp. 181–194. DOI: 10.3189/S0022143000021298.

Bindschadler, R. (1983). 'The Importance of Pressurized Subglacial Water in Separation and Sliding at the Glacier Bed'. eng. In: *Journal of glaciology* 29.101, pp. 3–19.

Björnsson, H. (Oct. 1998). 'Hydrological characteristics of the drainage system beneath a surging glacier'. In: *Nature* 395.6704, pp. 771–774. DOI: 10.1038/27384.

Björnsson, H. et al. (2003). 'Surges of glaciers in Iceland'. In: *Annals of Glaciology* 36, pp. 82–90. DOI: 10.3189/172756403781816365.

Björnsson, H. K. et al. (1996). 'The thermal regime of sub-polar glaciers mapped by multi-frequency radio-echo sounding'. In: *Journal of Glaciology* 42, pp. 23–32.

Błaszczyk, M., Jania, J. and Hagen, J. (Jan. 2009). 'Tidewater Glaciers of Svalbard: Recent changes and estimates of calving fluxes'. In: *Polish Polar Research* 30.

Bolch, T. et al. (2010). 'A glacier inventory for the western Nyainqentanglha Range and the Nam Co Basin, Tibet, and glacier changes 1976–2009'. In: *The Cryosphere* 4.3, pp. 419–433. DOI: 10.5194/tc-4-419-2010.

Bouchayer, C. et al. (2023). 'Multi-scale variations of hydro-mechanical conditions at the base of the surge-type glacier Kongsvegen, Svalbard'. In: *EGUsphere* 2023, pp. 1–41. DOI: 10.5194/egusphere-2023-618.

Bouchayer, C. et al. (2022). 'Observing the on-going destabilisation of an Arctic surge-type glacier, Kongsvegen.' In: *AGU Fall Meeting Abstracts*. Vol. 2022, C45E–1135.

Boulton, G. and Hindmarsh, R. C. A. (1987). 'Sediment deformation beneath glaciers: Rheology and geological consequences'. In: *Journal of Geophysical Research* 92, pp. 9059–9082.

Chudley, T. R. et al. (2022). 'Empirical correction of systematic orthorectification error in Sentinel-2 velocity fields for Greenlandic outlet glaciers'. In: *The Cryosphere* 16.6, pp. 2629–2642. DOI: 10.5194/tc-16-2629-2022.

Clarke, G. K. (1987). 'Fast glacier flow: ice streams, surging, and tidewater glaciers'. In: *Journal of Geophysical Research* 92.B9, pp. 8835–8841. DOI: 10.1029/JB092iB09p08835.

– (1991). 'Length, width and slope influences on glacier surging'. In: *Journal of Glaciology* 37.126, pp. 236–346. DOI: 10.1017/s0022143000007255.

Clarke, G. K. C., Collins, S. G. and Thompson, D. E. (1984). 'Flow, thermal structure, and subglacial conditions of a surge-type glacier'. In: *Canadian Journal of Earth Sciences* 21.2, pp. 232–240. DOI: 10.1139/e84-024. eprint: https://doi.org/10.1139/e84-024.

Clarke, G. K. (1976). 'Thermal Regulation of Glacier Surging'. In: *Journal of Glaciology* 16.74, pp. 231–250. DOI: 10.1017/s0022143000031567.

Constable, A. J. et al. (2022). 'Climate change 2022: Impacts, adaptation and vulnerability: Cross-chapter paper 6: Polar regions'. In: *Cambridge University Press, Cambridge, UK and New York, NY, USA*. DOI: 10.1017/9781009325844.023..

De Lange, R., Luckman, A. and Murray, T. (2007). 'Improvement of satellite radar feature tracking for ice velocity derivation by spatial frequency filtering'. In: *IEEE Transactions on Geoscience and Remote Sensing* 45.7, pp. 2309–2318. DOI: 10.1109/TGRS.2007.896615.

Debella-Gilo, M. and Kääb, A. (2012). 'Locally adaptive template sizes for matching repeat images of Earth surface mass movements'. In: *ISPRS Journal of Photogrammetry and Remote Sensing* 69, pp. 10–28. DOI: https://doi.org/10.1016/j.isprsjprs.2012.02.002.

Donghui, S. et al. (2016). 'Characterizing the May 2015 Karayaylak Glacier surge in the eastern Pamir Plateau using remote sensing'. In: *Journal of Glaciology* 62.235, pp. 944–953. DOI: 10.1017/jog.2016.81.

Dowdeswell, J. A. et al. (1995). 'Mass balance change as a control on the frequency and occurrence of glacier surges in Svalbard, Norwegian High Arctic'. In: *Geophysical Research Letters* 22.21, pp. 2909–2912. DOI: 10.1029/95GL02821.

Dowdeswell, J. A. and Benham, T. J. (2003). 'A surge of Perseibreen, Svalbard, examined using aerial photography and ASTER high resolution satellite imagery'. In: *Polar Research* 22.2, pp. 373–383. DOI: https://doi.org/10.1111/j.1751-8369.2003.tb00118.x. eprint: https://onlinelibrary.wiley.com/doi/pdf/10.1111/j.1751-8369.2003.tb00118.x.

Dowdeswell, J. A., Hamilton, G. S. and Hagen, J. O. (1991). 'The duration of the active phase on surge-type glaciers: contrasts between Svalbard and other regions'. In: *Journal of Glaciology* 37.127, pp. 388–400. DOI: 10.3189/s0022143000005827.

Eisen, O., Harrison, W. and Raymond, C. (June 2001). 'The surges of Variegated Glacier, Alaska, U.S.A., and their connection to climate and mass balance'. In: *Journal of Glaciology* 47, pp. 351–358. DOI: 10.3189/172756501781832179.

Eisen, O. et al. (2005). 'Variegated Glacier, Alaska, USA: a century of surges'. In: *Journal of Glaciology* 51.174, pp. 399–406. DOI: 10.3189/172756505781829250.

Fahnestock, M. et al. (2016). 'Rapid large-area mapping of ice flow using Landsat 8'. In: *Remote Sensing of Environment* 185, pp. 84–94. DOI: 10.1016/j.rse.2015.11.023.

Farmer, D. M. and Freeland, H. J. (1983). 'The physical oceanography of Fjords'. In: *Progress in Oceanography* 12.2, pp. 147–220. DOI: 10.1016/0079-6611(83)90004-6.

Flowers, G. E. (2015). 'Modelling water flow under glaciers and ice sheets'. In: *Proceedings of the Royal Society A: Mathematical, Physical and Engineering Sciences* 471.2176, p. 20140907. DOI: 10.1098/rspa.2014.0907. eprint: https://royalsocietypublishing.org/doi/pdf/10.1098/rspa.2014.0907.

Førland, E., Hanssen-Bauer, I. and Nordli, P. (1997). 'Climate statistics and longterm series of temperature and precipitation at Svalbard and Jan Mayen'. In: *Det Norske Meteorologiske Institutt Klima Report* 21, p. 97.

Fowler, A. C., Murray, T. and Ng, F. S. (2001). 'Thermally controlled glacier surging'. In: *Journal of Glaciology* 47.159, pp. 527–538. DOI: 10.3189/172756501781831792.

Frappé, T. P. and Clarke, G. K. (2007). 'Slow surge of Trapridge Glacier, Yukon Territory, Canada'. In: *Journal of Geophysical Research: Earth Surface* 112.3, pp. 1–17. DOI: 10.1029/2006JF000607.

Gardner, A. S. et al. (2018). 'Increased West Antarctic and unchanged East Antarctic ice discharge over the last 7 years'. In: *The Cryosphere* 12.2, pp. 521–547. DOI: 10.5194/tc-12-521-2018.

Geyman, E. C. et al. (2022). 'Historical glacier change on Svalbard predicts doubling of mass loss by 2100'. In: *Nature* 601.7893, pp. 374–379. DOI: 10.1038/s41586-021-04314-4.

Glen, J. W. (1955). 'The creep of polycrystalline ice'. In: *Proceedings of the Royal Society of London. Series A. Mathematical and Physical Sciences* 228.1175, pp. 519–538.

Goldstein, R. M. et al. (1993). 'Satellite Radar Interferometry for Monitoring Ice Sheet Motion: Application to an Antarctic Ice Stream'. In: *Science* 262.5139, pp. 1525–1530.

Hanelt, D. et al. (2001). 'Light regime in an Arctic fjord: A study related to stratospheric ozone depletion as a basis for determination of UV effects on algal growth'. In: *Marine Biology* 138.3, pp. 649–658. DOI: 10.1007/s002270000481.

Harrison, W. et al. (Jan. 1994). 'The 1987–88 surge of West Fork Glacier, Susitna Basin, Alaska, U.S.A.' In: *Journal of Glaciology* 40, pp. 241–254. DOI: 10.1017/S0022143000007334.

Harrison, W. D. and Post, A. S. (2003). 'How much do we really know about glacier surging?' In: *Annals of Glaciology* 36, pp. 1–6. DOI: 10.3189/172756403781816185.

Heid, T. and Kääb, A. (2012). 'Evaluation of existing image matching methods for deriving glacier surface displacements globally from optical satellite imagery'. In: *Remote Sensing of Environment* 118, pp. 339–355. DOI: 10.1016/j.rse.2011.11.024.

Herman, F., Anderson, B. and Leprince, S. (2011). 'Mountain glacier velocity variation during a retreat/advance cycle quantified using sub-pixel analysis of aster images'. In: *Journal of Glaciology* 57.202, pp. 197–207. DOI: 10.3189/002214311796405942.

Herreid, S. and Truffer, M. (2016). 'Automated detection of unstable glacier flow and a spectrum of speedup behavior in the Alaska Range'. In: *Journal of Geophysical Research: Earth Surface* 121.1, pp. 64–81.

Hewitt, K. (2014). *Glaciers of the Karakoram Himalaya*. Springer.

Hoinkes, H. C. (1969). 'Surges of the Vernagtferner in the Ötztal Alps since 1599'. In: *Canadian Journal of Earth Sciences* 6.4, pp. 853–861. DOI: 10.1139/e69-086.

Huang, L. and Li, Z. (2011). 'Comparison of SAR and optical data in deriving glacier velocity with feature tracking'. In: *International Journal of Remote Sensing* 32.10, pp. 2681–2698. DOI: 10.1080/01431161003720395. eprint: https://doi.org/10.1080/01431161003720395.

Ingolfsson, O. (2000). 'Outline of the geography and geology of Svalbard'. In: p. 12.

Ingólfsson, Ó. et al. (2016). 'Glacial geological studies of surge-type glaciers in Iceland — Research status and future challenges'. In: *Earth-Science Reviews* 152, pp. 37–69. DOI: https://doi.org/10.1016/j.earscirev.2015.11.008.

Jiskoot, H. (Jan. 2011). 'Dynamics of Glaciers'. In: pp. 245–256. DOI: 10.1007/978-90-481-2642-2_127.

Jiskoot, H., Boyle, P. and Murray, T. (1998). 'The incidence of glacier surging in Svalbard: evidence from multivariate statistics'. In: *Computers and Geosciences* 24.4, pp. 387–399. DOI: 10.1016/S0098-3004(98)00033-8.

Jiskoot, H., Murray, T. and Luckman, A. (2003). 'Surge potential and drainage-basin characteristics in East Greenland'. In: *Annals of Glaciology* 36, pp. 142–148. DOI: 10.3189/172756403781816220.

Kääb, A. (2005a). 'Remote sensing of mountain glaciers and permafrost creep, Schriftenreihe Physiche Geographie Glaziologie und Geomorphodynamik'. In: *Geographisches Institut der Universität Zürich*.

– (2005b). 'Combination of SRTM3 and repeat ASTER data for deriving alpine glacier flow velocities in the Bhutan Himalaya'. In: *Remote Sensing of Environment* 94.4, pp. 463–474. DOI: https://doi.org/10.1016/j.rse.2004.11.003.

Kääb, A. and Vollmer, M. (2000). 'Surface geometry, thickness changes and flow fields on creeping mountain permafrost: Automatic extraction by digital image analysis'.

In: *Permafrost and Periglacial Processes* 11.4, pp. 315–326. DOI: 10.1002/1099-1530(200012)11:4<315::AID-PPP365>3.0.CO;2-J.

Kääb, A. et al. (2021). 'Sudden large-volume detachments of low-angle mountain glaciers – more frequent than thought?' In: *The Cryosphere* 15.4, pp. 1751–1785. DOI: 10.5194/tc-15-1751-2021.

Kääb, A., Lefauconnier, B. and Melvold, K. (2005). 'Flow field of Kronebreen, Svalbard, using repeated Landsat 7 and ASTER data'. In: *Annals of Glaciology* 42.August, pp. 7–13. DOI: 10.3189/172756405781812916.

Kääb, A. et al. (2016). 'Glacier Remote Sensing Using Sentinel-2. Part I: Radiometric and Geometric Performance, and Application to Ice Velocity'. In: *Remote Sensing* 8.7. DOI: 10.3390/rs8070598.

Kamb, B. and Engelhardt, H. F. (1987). 'Waves of Accelerated Motion in a Glacier Approaching Surge: the Mini-Surges of Variegated Glacier, Alaska, U.S.A.' In: *Journal of Glaciology* 33, pp. 27–46. DOI: 10.3189/S0022143000005311.

Kamb, B. et al. (1985). 'Glacier surge mechanism: 1982-1983 surge of variegated glacier, Alaska'. In: *Science* 227.4686, pp. 469–479. DOI: 10.1126/science.227.4686.469.

Killie, M. A. et al. (Jan. 2021). *Svalbard snow and sea-ice cover: comparing satellite data, on-site measurements, and modelling results (SvalSCESIA)*. DOI: 10.5281/zenodo.4293804.

King, O., Bhattacharya, A. and Bolch, T. (2021). 'The presence and influence of glacier surging around the Geladandong ice caps, North East Tibetan Plateau'. In: *Advances in Climate Change Research* 12.3, pp. 299–312. DOI: https://doi.org/10.1016/j.accre.2021.05.001.

Koch, M. et al. (2023). 'Automated Detection of Glacier Surges from Sentinel-1 Surface Velocity Time Series - An Example from Svalbard'. In: *Remote Sensing* 15.6. DOI: 10.3390/rs15061545.

Köhler, A. et al. (2012). 'Autonomous detection of calving-related seismicity at Kronebreen, Svalbard'. In: *The Cryosphere* 6.2, pp. 393–406. DOI: 10.5194/tc-6-393-2012.

Lamont, J. and Livesay, W. (1876). *Yachting in the Arctic Seas*. Chatto and Windus.

Leclercq, P. W., Kääb, A. and Altena, B. (2021). 'Brief communication: Detection of glacier surge activity using cloud computing of Sentinel-1 radar data'. In: *The Cryosphere* 15.10, pp. 4901–4907. DOI: 10.5194/tc-15-4901-2021.

Lefauconnier, B. (1992). 'Recent fluctuations of glaciers in Kongsfjorden, Spitsbergen, Svalbard (79 N)'. In: *Polar Geography* 16.3, pp. 226–233.

Leinss, S., Round, V. and Hajnsek, I. (July 2017). 'Single pass InSAR missions for monitoring hazardous surging glaciers'. In: pp. 934–937. DOI: 10.1109/IGARSS.2017.8127106.

Liestøl, O. (1988). 'The glaciers in the Kongsfjorden area, Spitsbergen'. In: *Norsk Geografisk Tidsskrift - Norwegian Journal of Geography* 42.4, pp. 231–238. DOI: 10.1080/00291958808552205.

Lindbäck, K. et al. (2018). 'Subglacial topography , geomorphology and future bathymetry of Kongsfjorden , northwestern Svalbard'. In: *Unpublished manuscript*, pp. 1–51.

Lingle, C. S. and Fatland, D. R. (2003). 'Does englacial water storage drive temperate glacier surges?' In: *Annals of Glaciology* 36, pp. 14–20. DOI: 10.3189/172756403781816464.

Lønne, I. (Jan. 2016). 'A new concept for glacial geological investigations of surges, based on High-Arctic examples (Svalbard)'. In: *Quaternary Science Reviews* 132, pp. 74–100. DOI: 10.1016/j.quascirev.2015.11.009.

Luckman, A., Murray, T. and Strozzi, T. (2002). 'Surface flow evolution throughout a glacier surge measured by satellite radar interferometry'. In: *Geophysical Research Letters* 29.23, pp. 2–5. DOI: 10.1029/2001GL014570.

Luckman, A., Quincey, D. and Bevan, S. (2007). 'The potential of satellite radar interferometry and feature tracking for monitoring flow rates of Himalayan glaciers'. In: *Remote Sensing of Environment* 111.2. Remote Sensing of the Cryosphere Special Issue, pp. 172–181. DOI: https://doi.org/10.1016/j.rse.2007.05.019.

Luckman, A. et al. (2015). 'Calving rates at tidewater glaciers vary strongly with ocean temperature'. In: *Nature Communications* 6. DOI: 10.1038/ncomms9566.

Meier, M. F. and Post, A. (1969). 'What are glacier surges?' In: *Canadian Journal of Earth Sciences* 6.4, pp. 807–817. DOI: 10.1139/e69-081. eprint: https://doi.org/10.1139/e69-081.

Melvold, K. (1998). 'Evolution of a surge-type glacier in its quiescent phase: Kongsvegen, Spitsbergen, 1964-95'. In: *Journal of Glaciology* 44.147, pp. 394–404. DOI: 10.1017/S0022143000002720.

Millan, R. et al. (2019). 'Mapping Surface Flow Velocity of Glaciers at Regional Scale Using a Multiple Sensors Approach'. In: *Remote Sensing* 11.21. DOI: 10.3390/rs11212498.

Mukherjee, K. et al. (2017). 'Surge-Type Glaciers in the Tien Shan (Central Asia)'. In: *Arctic, Antarctic, and Alpine Research* 49.1, pp. 147–171. DOI: 10.1657/AAAR0016-021.

Murray, T. (1998). 'Geometric evolution and ice dynamics during a surge of Bakaninbreen, Svalbard'. In: *Journal of Glaciology* 44.147, pp. 263–272. DOI: 10.1017/S0022143000002604.

Murray, T. and Porter, P. R. (2001). 'Basal conditions beneath a soft-bedded polythermal surge-type glacier: Bakaninbreen, Svalbard'. In: *Quaternary International* 86.1. Glacier Bed-Deforming Processes, pp. 103–116. DOI: https://doi.org/10.1016/S1040-6182(01)00053-2.

Murray, T. et al. (2000). 'Glacier surge propagation by thermal evolution at the bed'. In: *Journal of Geophysical Research: Solid Earth* 105.B6, pp. 13491–13507. DOI: https://doi.org/10.1029/2000JB900066. eprint: https://agupubs.onlinelibrary.wiley.com/doi/pdf/10.1029/2000JB900066.

Murray, T. et al. (2003a). 'Is there a single surge mechanism? Contrasts in dynamics between glacier surges in Svalbard and other regions'. In: *Journal of Geophysical Research: Solid Earth* 108.B5. DOI: 10.1029/2002jb001906.

Murray, T. et al. (2003b). 'The initiation of glacier surging at Fridtjovbreen, Svalbard'. In: *Annals of Glaciology* 36, pp. 110–116. DOI: 10.3189/172756403781816275.

Nagy, T. et al. (2019). 'SenDiT: The sentinel-2 displacement toolbox with application to glacier surface velocities'. In: *Remote Sensing* 11.10, pp. 1–21. DOI: 10.3390/rs11101151.

Narama, C. et al. (2010). 'Spatial variability of recent glacier area changes in the Tien Shan Mountains, Central Asia, using Corona (1970), Landsat (2000), and ALOS (2007) satellite data'. In: *Global and Planetary Change* 71.1, pp. 42–54. DOI: https://doi.org/10.1016/j.gloplacha.2009.08.002.

Nuth, C. et al. (2013). 'Decadal changes from a multi-temporal glacier inventory of Svalbard'. In: *Cryosphere* 7.5, pp. 1603–1621. DOI: 10.5194/tc-7-1603-2013.

Nuth, C. et al. (2010). 'Svalbard glacier elevation changes and contribution to sea level rise'. In: *Journal of Geophysical Research: Earth Surface* 115.F1. DOI: https://doi.org/10.1029/2008JF001223. eprint: https://agupubs.onlinelibrary.wiley.com/doi/pdf/10.1029/2008JF001223.

Nuth, C. et al. (2012). 'Estimating the long-term calving flux of Kronebreen, Svalbard from geodetic elevation changes and mass-balance modelling'. In: *Journal of Glaciology* 58.207, pp. 119–133. DOI: 10.3189/2012JoG11J036.

Nye, J. F. (Feb. 1957). 'The Distribution of Stress and Velocity in Glaciers and Ice-Sheets'. In: *Proceedings of the Royal Society of London Series A* 239.1216, pp. 113–133. DOI: 10.1098/rspa.1957.0026.

Paterson, W. (1994). *Physics of Glaciers*. Elsevier Science.

Paul, F. et al. (2022). 'Three different glacier surges at a spot: what satellites observe and what not'. In: *The Cryosphere* 16.6, pp. 2505–2526. DOI: 10.5194/tc-16-2505-2022.

Paul, F. et al. (2015). 'The glaciers climate change initiative: Methods for creating glacier area, elevation change and velocity products'. In: *Remote Sensing of Environment* 162, pp. 408–426. DOI: https://doi.org/10.1016/j.rse.2013.07.043.

Pavlova, O., Gerland, S. and Hop, H. (2019). 'Changes in Sea-Ice Extent and Thickness in Kongsfjorden, Svalbard (2003–2016)'. In: *The Ecosystem of Kongsfjorden, Svalbard*. Ed. by Hop, H. and Wiencke, C. Cham: Springer International Publishing, pp. 105–136. DOI: 10.1007/978-3-319-46425-1_4.

Placidi, L., Hutter, C. and Faria, S. (Apr. 2006). 'A Critical Review of the Mechanics of Polycrystalline Polar Ice'. In: *GAMM-Mitteilungen* 29. DOI: 10.1002/gamm.201490025.

Post, A. (1969). 'Distribution of Surging Glaciers in Western North America'. In: *Journal of Glaciology* 8.53, pp. 229–240. DOI: 10.3189/S0022143000031221.

Post, A. S. (Apr. 1965). 'Alaskan Glaciers: Recent Observations in Respect to the Earthquake-Advance Theory'. In: *Science* 148.3668, pp. 366–368. DOI: 10.1126/science.148.3668.366.

Quincey, D. and Glasser, N. (2009). 'Morphological and ice-dynamical changes on the Tasman Glacier, New Zealand, 1990–2007'. In: *Global and Planetary Change* 68.3, pp. 185–197. DOI: https://doi.org/10.1016/j.gloplacha.2009.05.003.

Rao, Y. S. (2011a). 'Synthetic Aperture Radar (SAR) Interferometry for Glacier Movement Studies'. In: *Encyclopedia of Snow, Ice and Glaciers*. Ed. by Singh, V. P., Singh, P. and Haritashya, U. K. Dordrecht: Springer Netherlands, pp. 1133–1142. DOI: 10.1007/978-90-481-2642-2_618.

– (2011b). 'Synthetic Aperture Radar (SAR) Interferometry for Glacier Movement Studies'. In: *Encyclopedia of Snow, Ice and Glaciers*. Ed. by Singh, V. P., Singh, P. and Haritashya, U. K. Dordrecht: Springer Netherlands, pp. 1133–1142. DOI: 10.1007/978-90-481-2642-2_618.

Raup, B. H. et al. (2015). 'Remote sensing of glaciers'. In: *Remote Sensing of the Cryosphere*. John Wiley & Sons, Ltd. Chap. 7, pp. 123–156. DOI: https://doi.org/

10.1002/9781118368909.ch7. eprint: https://onlinelibrary.wiley.com/doi/pdf/10.1002/9781118368909.ch7.

Raymond, C., Johannesson, T. and Pfeffer, T. (1987). 'Propagation of a glacier surge into stagnant ice'. In: *Journal of Geophysical Research* 92.B9, pp. 9037–9049. DOI: 10.1029/JB092iB09p09037.

Reger, R. D. (1991). 'Short Notes on Alaskan Geology 1991'. In: p. 104.

Rolstad, C. et al. (1997). 'Visible and near-infrared digital images for determination of ice velocities and surface elevation during a surge on Osbornebreen, a tidewater glacier in Svalbard'. In: *Annals of Glaciology* 24, pp. 255–261. DOI: 10.1017/s026030550001226x.

Roy, D. et al. (2014). 'Landsat-8: Science and product vision for terrestrial global change research'. In: *Remote Sensing of Environment* 145, pp. 154–172. DOI: https://doi.org/10.1016/j.rse.2014.02.001.

Scambos, T. A. et al. (1992). 'Application of image cross-correlation to the measurement of glacier velocity using satellite image data'. In: *Remote sensing of environment* 42.3, pp. 177–186.

Schellenberger, T. et al. (2015). 'Surface speed and frontal ablation of Kronebreen and Kongsbreen, NW Svalbard, from SAR offset tracking'. In: *Cryosphere* 9.6, pp. 2339–2355. DOI: 10.5194/tc-9-2339-2015.

Schild, K. M. et al. (2018). 'Glacier Calving Rates Due to Subglacial Discharge, Fjord Circulation, and Free Convection'. In: *Journal of Geophysical Research: Earth Surface* 123.9, pp. 2189–2204. DOI: 10.1029/2017JF004520.

Scholzen, C., Schuler, T. V. and Gilbert, A. (2021). 'Sensitivity of subglacial drainage to water supply distribution at the Kongsfjord basin, Svalbard'. In: *Cryosphere* 15.6, pp. 2719–2738. DOI: 10.5194/tc-15-2719-2021.

Schuler, T. V. et al. (2020). 'Reconciling Svalbard Glacier Mass Balance'. In: *Frontiers in Earth Science* 8.May, pp. 1–16. DOI: 10.3389/feart.2020.00156.

Selley, R., Cocks, L. and Plimer, I. (2005). *Encyclopedia of Geology*. Encyclopedia of Geology v. 1. Elsevier Academic.

Sevestre, H. and Benn, D. I. (2015). 'Climatic and geometric controls on the global distribution of surge-type glaciers: Implications for a unifying model of surging'. In: *Journal of Glaciology* 61.228, pp. 646–662. DOI: 10.3189/2015JoG14J136.

Sevestre, H. et al. (2018). 'Tidewater Glacier Surges Initiated at the Terminus'. In: *Journal of Geophysical Research: Earth Surface* 123.5, pp. 1035–1051. DOI: 10.1029/2017JF004358.

Sexton, D. J. et al. (1992). 'Seismic architecture and sedimentation in northwest Spitsbergen fjords'. In: *Marine Geology* 103.1-3, pp. 53–68. DOI: 10.1016/0025-3227(92)90008-6.

Sharp, M. (1985). 'Surging glaciers : behaviour and mechanisms by Martin Sharp'. In: 1969.

Singh, R. M. et al. (2021). 'Characterizing the glacier surge dynamics in Yarkand basin, Karakoram using remote sensing'. In: *Quaternary International* 575-576. SI: Remote Sensing and GIS Applications in Quaternary Sciences, pp. 190–203. DOI: https://doi.org/10.1016/j.quaint.2020.06.042.

Strozzi, T. et al. (2002). 'Glacier motion estimation using SAR offset-tracking procedures'. In: *IEEE Transactions on Geoscience and Remote Sensing* 40.11, pp. 2384–2391. DOI: 10.1109/TGRS.2002.805079.

Sun, Z. and Qiao, G. (2021). 'A REVIEW OF SURGE-TYPE GLACIERS'. In: XLIII, pp. 503–508.

Svendsen, H. et al. (2002). 'The physical environment of Kongsfjorden-Krossfjorden, and Arctic fjord system in Svalbard'. In: *Polar Research* 21.1, pp. 133–166. DOI: 10.1111/j.1751-8369.2002.tb00072.x.

Syvitski, J. P. (1989). 'On the deposition of sediment within glacier-influenced fjords: Oceanographic controls'. In: *Marine Geology* 85.2-4, pp. 301–329. DOI: 10.1016/0025-3227(89)90158-8.

Tarr, R. S. and Martin, L. (1914). *Alaskan Glacier Studies of the National Geographic Society in the Yakutat Bay, Prince William Sound and Lower Copper River Regions*. National Geographic Society.

Truffer, M. et al. (2021). *Glacier surges*, pp. 417–466. DOI: 10.1016/b978-0-12-817129-5.00003-2.

Trusel, L. D. et al. (2010). 'Modern glacimarine processes and potential future behaviour of Kronebreen and Kongsvegen polythermal tidewater glaciers, Kongsfjorden, Svalbard'. In: *Geological Society Special Publication* 344.November, pp. 89–102. DOI: 10.1144/SP344.9.

Vachon, P. et al. (1996). 'Differential SAR interferometry measurements of Athabasca and Saskatchewan glacier flow rate'. In: *Canadian Journal of Remote Sensing* 22.3, pp. 287–296.

Vallot, D. et al. (2017). 'Basal dynamics of Kronebreen, a fast-flowing tidewater glacier in Svalbard: Non-local spatio-Temporal response to water input'. In: *Journal of Glaciology* 63.242, pp. 1012–1024. DOI: 10.1017/jog.2017.69.

Van Wyk de Vries, M. and Wickert, A. D. (2021). 'Glacier Image Velocimetry: an open-source toolbox for easy and rapid calculation of high-resolution glacier velocity fields'. In: *The Cryosphere* 15.4, pp. 2115–2132. DOI: 10.5194/tc-15-2115-2021.

Veen, C. van der (2013). *Fundamentals of Glacier Dynamics, Second Edition*. Taylor & Francis.

Wang, C. et al. (Jan. 2021). 'Use of L-band SAR data for Monitoring Glacier Surging next to Aru Lake'. In: *Procedia Computer Science* 181, pp. 1131–1137. DOI: 10.1016/j.procs.2021.01.310.

Wang, Z. et al. (2023). 'Characteristics of Glaciers Surging in the Western Pamirs'. In: *Remote Sensing* 15.5. DOI: 10.3390/rs15051319.

Wendt, A. et al. (2017). 'A glacier surge of Bivachny Glacier, Pamir Mountains, observed by a time series of high-resolution digital elevation models and glacier velocities'. In: *Remote Sensing* 9.4, p. 388. DOI: 10.3390/rs9040388.

Wiencke, C. and Hop, H. (2016). *Ecosystem Kongsfjorden: new views after more than a decade of research*.

Yin, B. et al. (2019). 'Recent Kyagar glacier lake outburst flood frequency in Chinese Karakoram unprecedented over the last two centuries'. In: *Natural Hazards* 95, pp. 877–881.

Zemp, M. et al. (2019). 'Global glacier mass changes and their contributions to sea-level rise from 1961 to 2016'. In: *Nature* 568.7752, pp. 382–386. DOI: 10.1038/s41586-019-1071-0.